RESEARCH ARTICLE

KAT6A and ENL Form an Epigenetic Transcriptional Control Module to Drive Critical Leukemogenic Gene-Expression Programs

Fangxue Yan[1,2], Jinyang Li[2], Jelena Milosevic[3], Ricardo Petroni[1], Suying Liu[2,4], Zhennan Shi[5], Salina Yuan[2], Janice M. Reynaga[1], Yuwei Qi[2], Joshua Rico[1], Sixiang Yu[2,4], Yiman Liu[2,4,6], Susumu Rokudai[7], Neil Palmisiano[8], Sara E. Meyer[9], Pamela J. Sung[10], Liling Wan[2,4,6], Fei Lan[5], Benjamin A. Garcia[6], Ben Z. Stanger[2,11], David B. Sykes[3,12], and M. Andrés Blanco[1]

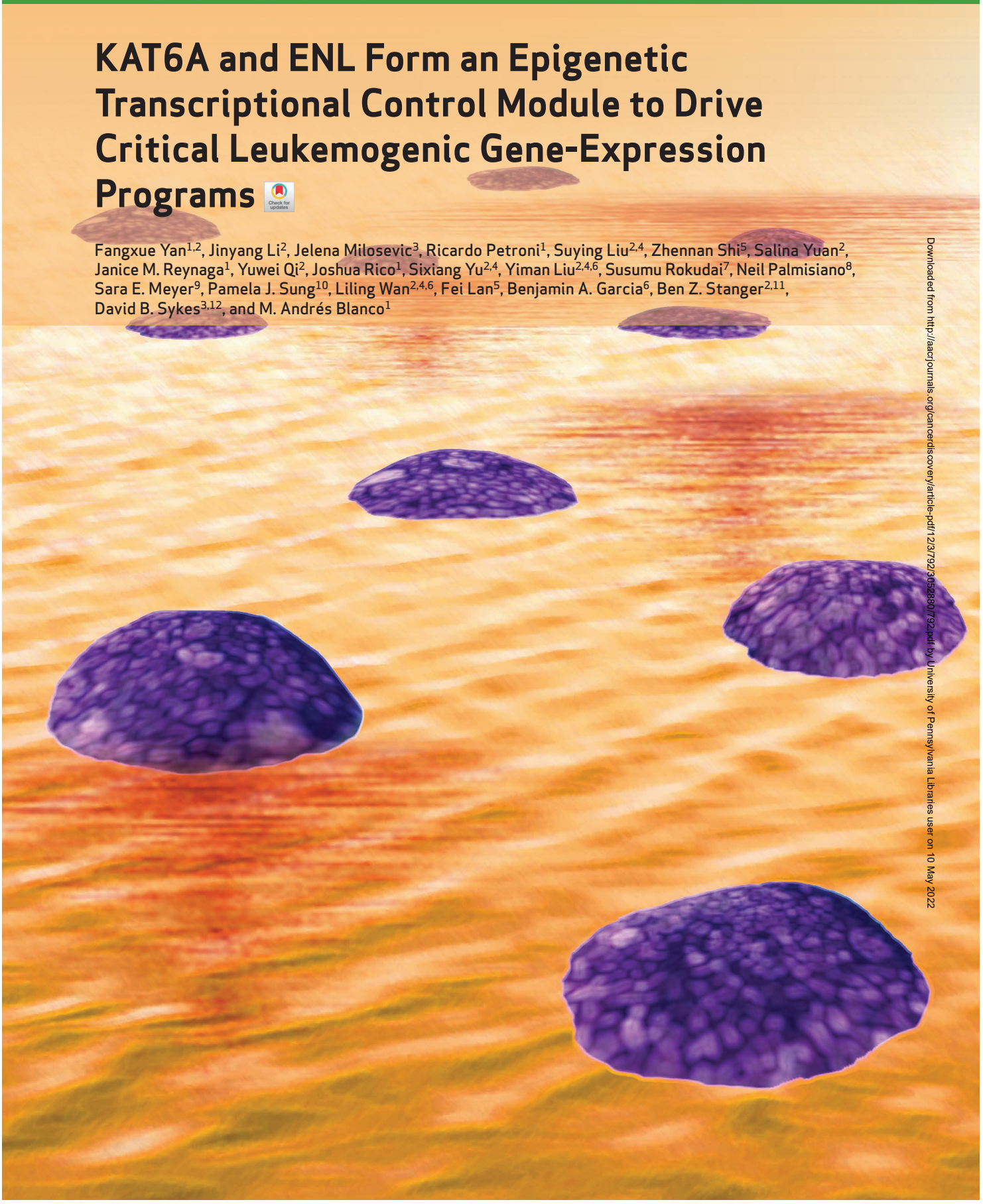

ABSTRACT Epigenetic programs are dysregulated in acute myeloid leukemia (AML) and help enforce an oncogenic state of differentiation arrest. To identify key epigenetic regulators of AML cell fate, we performed a differentiation-focused CRISPR screen in AML cells. This screen identified the histone acetyltransferase KAT6A as a novel regulator of myeloid differentiation that drives critical leukemogenic gene-expression programs. We show that KAT6A is the initiator of a newly described transcriptional control module in which KAT6A-catalyzed promoter H3K9ac is bound by the acetyl-lysine reader ENL, which in turn cooperates with a network of chromatin factors to induce transcriptional elongation. Inhibition of KAT6A has strong anti-AML phenotypes *in vitro* and *in vivo*, suggesting that KAT6A small-molecule inhibitors could be of high therapeutic interest for monotherapy or combinatorial differentiation-based treatment of AML.

SIGNIFICANCE: AML is a poor-prognosis disease characterized by differentiation blockade. Through a cell-fate CRISPR screen, we identified KAT6A as a novel regulator of AML cell differentiation. Mechanistically, KAT6A cooperates with ENL in a "writer–reader" epigenetic transcriptional control module. These results uncover a new epigenetic dependency and therapeutic opportunity in AML.

INTRODUCTION

Acute myeloid leukemia (AML) is one of the most deadly hematologic malignancies, and the majority of diagnosed patients will die from their disease (1, 2). Chemotherapy is standard of care, but therapeutic regimens have not changed dramatically in several decades and are often poorly tolerated (3). Accordingly, there is an outstanding need for novel AML treatments.

Although genetically heterogenous, all AMLs are characterized by differentiation blockade, which enables their continual self-renewal and proliferation (4–6). Although chemotherapy aims to eliminate AML cells by directly inducing cell death or cell-cycle arrest, differentiation therapy provides an alternative in which self-renewal is depleted by inducing myeloid maturation programs, thereby extinguishing proliferation (4). This approach is curative in the promyelocytic AML subtype (APL) and promising in *IDH*-mutant AMLs, but has not been successful in other subtypes (4, 7–9). To expand the applicability of differentiation therapy, it is critical to understand the mechanisms regulating AML cell-fate decisions.

Epigenetic regulators are of marked importance for sustaining the transcriptional programs that drive AML differentiation arrest (10, 11). In particular, numerous recent studies have highlighted the critical role of enhancer regulation in AML transcriptional control (12–15). For example, the acetyl-lysine–binding "reader" protein BRD4 is essential for maintaining the active state of enhancers and superenhancers that regulate the expression of AML oncogenes such as *MYC* (16–19). In contrast, the H3K4me1/2 histone demethylase LSD1/KDM1A silences genes driving myeloid differentiation by inactivating their enhancers (20–24). However, although AML enhancer regulation has been studied in depth in recent years, comparatively fewer studies are focusing on the equally important process of promoter state regulation.

A recent breakthrough in AML promoter regulation was made by parallel studies that identified the YEATS domain protein ENL/MLLT1 as an H3K9ac and H3K27ac histone acetyl-lysine reader that promotes oncogenic transcription in AML (25, 26). These studies uncovered an elegant chromatin regulatory "module" in which promoter-bound ENL recruits the super elongation complex to help release paused RNA Pol II and drive transcription of *MYC* and other AML oncogenes. Although these studies showed how "reading" of promoter states can provide instructions for transcriptional

[1]Department of Biomedical Sciences, School of Veterinary Medicine, University of Pennsylvania, Philadelphia, Pennsylvania. [2]Abramson Family Cancer Research Institute, Perelman School of Medicine, University of Pennsylvania, Philadelphia, Pennsylvania. [3]Center for Regenerative Medicine, Massachusetts General Hospital, Boston, Massachusetts. [4]Department of Cancer Biology, Perelman School of Medicine, University of Pennsylvania, Philadelphia, Pennsylvania. [5]Shanghai Key Laboratory of Medical Epigenetics, International Co-laboratory of Medical Epigenetics and Metabolism, Ministry of Science and Technology, Institutes of Biomedical Sciences, Fudan University, and Key Laboratory of Carcinogenesis and Cancer Invasion, Ministry of Education, Liver Cancer Institute, Zhongshan Hospital, Fudan University, Shanghai, China. [6]Penn Epigenetics Institute, Perelman School of Medicine, University of Pennsylvania, Philadelphia, Pennsylvania. [7]Department of Molecular Pharmacology and Oncology, Gunma University, Gunma, Japan. [8]Department of Medical Oncology, Thomas Jefferson University, Sidney Kimmel Cancer Center, Philadelphia, Pennsylvania. [9]Department of Cancer Biology, Thomas Jefferson University, Sidney Kimmel Cancer Center, Philadelphia, Pennsylvania. [10]Division of Hematology/Oncology, University of Pennsylvania, Philadelphia, Pennsylvania. [11]Department of Medicine, Perelman School of Medicine, University of Pennsylvania, Philadelphia, Pennsylvania. [12]Havard Stem Cell Institute, Cambridge, Massachusetts.

Note: Supplementary data for this article are available at Cancer Discovery Online (http://cancerdiscovery.aacrjournals.org/).

F. Yan, J. Li, and J. Milosevic contributed equally to this article.

Current address for P.J Sung: Department of Medicine, Roswell Park Comprehensive Cancer Center, Buffalo, New York.

Corresponding Authors: M. Andrés Blanco, University of Pennsylvania, Hill Pavilion H414, 380S University Avenue, Philadelphia, PA 19104. Phone: 609-647-6687; E-mail: ablanco@vet.upenn.edu; and David B. Sykes, dbsykes@mgh.harvard.edu

Cancer Discov 2022;12:792–811

doi: 10.1158/2159-8290.CD-20-1459

elongation, the critical initiators of this module—the "writers" that provide acetyl substrates for ENL binding—remain to be identified.

CRISPR screening has emerged as an exciting method for using genetic screening logic to identify regulators of diverse phenotypes in mammalian cells (27, 28). Several CRISPR "dropout" screens have been performed to identify regulators of AML cell survival and proliferation (29–32). Although effective for studies of cell growth and survival, these screens may miss the most critical regulators of AML cell fate.

Here, we designed a positive selection gain-of-differentiation CRISPR screen to identify chromatin regulators whose inhibition induces therapeutic differentiation of AML cells. This screen identified the H3K9 acetyltransferase KAT6A/MYST3/MOZ as a critical driver of AML stemness and proliferation. Through a combination of experimental and bioinformatic approaches, we show that KAT6A collaborates with ENL to drive a *MYC*-centric gene-expression program by providing promoter H3K9ac for ENL binding. This work establishes an actionable KAT6A–ENL axis with implications for non-APL AML differentiation therapy.

RESULTS

Epigenetic-Focused CRISPR–Cas9 Screen Identifies KAT6A as an AML Differentiation Regulator

To identify novel epigenetic regulators of AML differentiation arrest, we designed a CRISPR–Cas9 screen based on selection of CD11b, a surface marker of myeloid differentiation (Fig. 1A). We chose to use the human U937 cell line due to its large dynamic range of CD11b level and strong response to known differentiation inducers such as LSD1 inhibitors (21), making it a robust model for the initial identification of differentiation regulators. We transduced Cas9-expressing U937 cells with a custom single-guide RNA (sgRNA) library targeting 904 chromatin regulators and RNA-binding proteins. Nine days after transduction, cells were isolated by FACS based on surface CD11b expression. Live CD11b-high (most differentiated), CD11b-low (least differentiated), and unsorted reference (bulk) groups were collected and deep-sequenced to measure sgRNA representations (Supplementary Fig. S1A–S1C; Supplementary Table S1). Comparing CD11b-high and CD11b-low groups, we identified 73 and 56 genes significantly enriched in each population, respectively, using the MAGeCK robust ranking algorithm (RRA; ref. 33; Fig. 1B; Supplementary Fig. S1D; Supplementary Table S2). Strikingly, the top 14 hits identified in the CD11b-high group (corresponding to genes whose loss induces differentiation) all belong to genes encoding two protein complexes: the Mediator complex and LSD1/KDM1A-CoREST complexes, both of which are well-established repressors of AML differentiation (19–22). Other hits included EP300 and DOT1L, which have also been shown to have important roles in AML (34–36). These results confirm the validity of the screen and suggest that other high-scoring hits may represent novel differentiation regulators of significant importance for AML.

We focused on the histone acetyltransferase (HAT) KAT6A, a hit that has not been studied in depth in AML. Not only was KAT6A among the top-scoring genes in the differentiated (CD11b-high) group, SIRT1—a deacetylase that can remove the same modifications catalyzed by KAT6A—was among the top hits in the undifferentiated (CD11b-low) group (Fig. 1B; Supplementary Fig. S1E). As these two enzymes with opposing functions scored in the opposite phenotypic groups, we suspect that KAT6A/SIRT1-controlled histone acetylation might play an important role in regulating AML differentiation.

KAT6A (also known as MOZ, MYST3) is a MYST family HAT that can catalyze H3K9ac, H3K14ac, and H3K23ac (37, 38). Interestingly, chromosomal translocations that fuse *KAT6A* to other genes (such as *CREBBP/TIF2/EP300*) are found to be driver events in AML (39–41). However, the function of wild-type (WT) KAT6A in AML has not been reported. To gain insight into whether KAT6A has a role in AML development and differentiation arrest, we first analyzed RNA-sequencing (RNA-seq) data from The Cancer Genome Atlas (TCGA; ref. 42) and TARGET (43) clinical cancer sample data sets, as well as from cancer cell lines and normal human tissue using the Cancer Cell Line Encyclopedia (CCLE; ref. 44) and Genotype-Tissue Expression (GTEx; ref. 45) databases, respectively. Analyzing TCGA data, we found that *KAT6A* has the highest expression in acute myeloid leukemia (LAML) across all cancer types (Fig. 1C). Integrating GTEx and TCGA data, we also found that *KAT6A* expression is significantly higher in AML than in matched normal tissue (Fig. 1D). We then investigated transcriptional correlations between *KAT6A* and myeloid differentiation programs. Intriguingly, in the TCGA, TARGET, and CCLE databases, we observed that *KAT6A* high-expressing AML samples strongly repress the monocyte differentiation gene-expression signature (ref. 46; Fig. 1E). These results are consistent with a role for KAT6A in promoting AML via opposing myeloid differentiation.

We next validated the screen results in multiple human AML cell lines with diverse genetic alterations: U937 (*CALM-AF10* translocation), MOLM-13 and NOMO-1 (both *MLL–AF9* translocation), MV4;11 (*MLL–AF4* translocation), HL-60 (*MYC* amplified), and OCI-AML3 (*DNMT3A* and *NPM1* mutation).

Figure 1. CRISPR–Cas9 screen identifies KAT6A as a differentiation regulator in AML. **A,** Schematic outline of CRISPR–Cas9 screen. gDNA, genomic DNA; MOI, multiplicity of infection. **B,** Volcano plot showing the top hits enriched in CD11b-low (blue) or CD11b-high (red) populations, with $P < 0.05$. Several top hits in Mediator complex (purple) and LSD1–CoREST complex (green) are highlighted. **C,** *KAT6A* expression levels in cancer types from TCGA, using the Gene-Expression Profiling Interactive Analysis (GEPIA) online server. T, tumor/cancer; TPM, transcripts per million. **D,** Box plot comparing *KAT6A* expression levels between AML samples (from TCGA data set) and matched normal samples (from TCGA and GTEx projects), using the GEPIA online server. **E,** Leading-edge plot showing the enrichment of a monocyte differentiation gene set based on gene set enrichment analysis of *KAT6A* high-expressing (top 20%) and *KAT6A* low-expressing (bottom 20%) AML samples from TCGA (left), TARGET (center), and CCLE (right) data sets. ES, enrichment score; FDR, false discovery rate. **F,** Surface expression of CD11b after lentiviral transduction of empty vector and sgRNAs targeting KAT6A (sgKAT6A-1 and sgKAT6A-2) in U937 cells on day 9 ($n = 2$–4 in each group). MFI, mean fluorescence intensity. **G,** Surface expression of CD11b after lentiviral transduction of empty vector and sgRNAs targeting KAT6A (sgKAT6A-1 and sgKAT6A-2) in MOLM-13 cells on indicated days ($n = 2$–4 each group). **H,** Representative flow cytometry histogram of surface CD11b expression in MOLM-13 cells on day 9. **I,** Functional change in myeloid differentiation in MOLM-13 cells as measured by superoxide anion production. Statistical differences were calculated using an unpaired Student *t* test (**D** and **F**) and multiple *t* test (**G**). All error bars represent mean ± SD, and $P < 0.05$ was considered statistically significant; *, $P < 0.05$; **, $P < 0.01$. See also Supplementary Fig. S1.

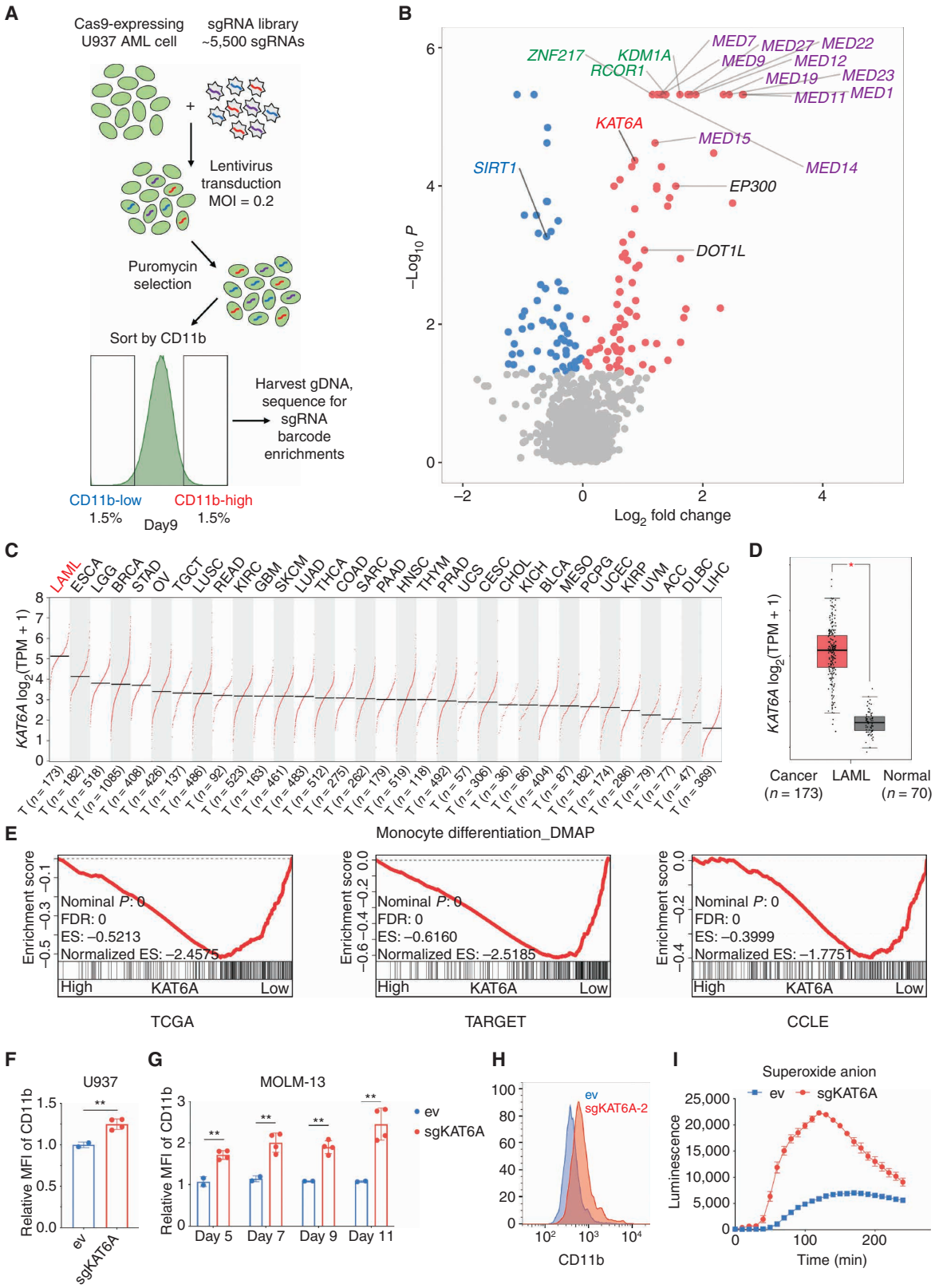

Depletion of *KAT6A* by sgKAT6A was confirmed by sequencing of the *KAT6A* locus (Supplementary Fig. S1F) and qPCR of *KAT6A* expression (Supplementary Fig. S1G). In all cases, surface expression of CD11b was increased upon depletion of KAT6A, indicating that screen results were not unique to U937 cells and that KAT6A may contribute to the AML differentiation block in a broad spectrum of AML backgrounds (Fig. 1F–H; Supplementary Fig. S1H). Upregulation of surface CD86 was also confirmed following loss of KAT6A (Supplementary Fig. S1I and S1J). To validate functional cellular differentiation, we also observed a strong induction of superoxide anion production following KAT6A depletion (Fig. 1I).

Together, these results suggest that KAT6A is a newly identified AML differentiation regulator.

Loss of KAT6A Impairs AML Stemness and Proliferation *In Vitro* and *In Vivo*

To further confirm the role of KAT6A in blocking differentiation, we used more functional assays for mitotic capacity and self-renewal. First, we tested whether KAT6A is a proliferation requirement in AML cells using negative-selection long-term growth competition assays. Human AML cell lines were transduced with GFP-expressing sgRNA vectors, and the ratio of GFP^+ (transduced) to GFP^- (nontransduced reference) cells was determined over three weeks (Fig. 2A). Intriguingly, we found that in all three MLL-rearranged (MLL-r) cell lines used, sgKAT6A-expressing cells were dramatically outcompeted by *KAT6A*-WT cells. The phenotype in MLL-r cells was even stronger than in U937 cells that were used for the screen, in which sgKAT6A-expressing cells were outcompeted significantly but more gradually. In OCI-AML3 and HL-60 cells, which are also MLL WT, KAT6A depletion had minimal effects on proliferation. This is in line with results from a recently published series of genome-wide CRISPR–Cas9 screens in 14 human AML cell lines (30) in which loss of KAT6A, along with several other subunits of the KAT6A complex, was significantly more deleterious in MLL-r compared with MLL-WT AML cells (Supplementary Fig. S2A).

We evaluated the role of KAT6A in MLL-r AML in more depth. Consistent with the proliferation phenotypes, we found that loss of KAT6A induced cell-cycle arrest (Fig. 2B) and moderately elevated apoptosis levels in the MLL-r cell lines MOLM-13 and MV4;11 (Supplementary Fig. S2B). Importantly, KAT6A depletion also markedly impaired clonogenic potential of MOLM-13 cells, confirming the importance of KAT6A in self-renewal (Fig. 2C). KAT6A is known to inhibit senescence via the INK4A–ARF pathway (47, 48). Consistent with these studies, we also observed that loss of KAT6A induced an increase in β-galactosidase activity—a marker of senescence (Fig. 2D).

We then tested the effect of KAT6A depletion on AML progression *in vivo*. We transduced luciferase-GFP–labeled MOLM-13 cells with mCherry-linked sgKAT6A or empty vector constructs, and 48 hours later isolated successfully transduced cells (GFP^+ $mCherry^+$) via FACS and injected them into sublethally irradiated NOD/SCID/gamma (NSG) mice. Leukemic burden was then quantified every two to four days by *in vivo* bioluminescent imaging. Up to six days after injection, no differences in disease progression were observed between mice receiving control and *KAT6A*-knockout (KO) cells, suggesting their equivalent engraftment and initial *in vivo* growth (Supplementary Fig. S2C). However, after day 6, *KAT6A*-KO cell growth slowed significantly, and disease burden lagged progressively more behind mice receiving control cells until endpoints were reached (Fig. 2E and F). Notably, leukemia cells recovered from sgKAT6A mice at the experiment endpoint were found to be around 70% mCherry negative, corresponding to nontransduced, *KAT6A*-WT cells (Supplementary Fig. S2D). In contrast, only less than 5% of the originally injected cells were mCherry negative (cells that inadvertently passed the mCherry-positive FACS gate). This suggests that disease burden in sgKAT6A mice was in fact primarily generated by more rapidly growing *KAT6A*-WT cells. Ultimately, KAT6A depletion significantly extended mouse survival (Fig. 2G), confirming that the importance of KAT6A in AML is conserved *in vivo*.

To expand our findings to primary mouse models, we also validated the role of KAT6A in Cas9-expressing mouse MLL–AF9 cells, a cell line generated by retroviral transduction of *Mll–Af9* fusion gene in mouse bone marrow cells. Similar to human MLL-r cells, sgKat6a mouse cells were outcompeted by WT cells in a competition assay (Fig. 2H) and showed impaired clonogenic potential (Fig. 2I), while an MLL-WT mouse primary cell model, Cas9–AML1-ETO (49), was not sensitive to KAT6A depletion (Supplementary Fig. S2E). After *in vivo* transplantation of mouse MLL–AF9 cells, we also observed a remarkable delay in leukemia progression in mice receiving *Kat6a*-KO cells (Fig. 2J).

Taken together, these results suggest that KAT6A is important for maintaining AML both *in vitro* and *in vivo*.

Enzymatic Function of KAT6A Is Required for AML Growth

As an acetyltransferase, the role of KAT6A in AML could be dependent on its enzymatic activity, its structural function,

Figure 2. KAT6A is required for AML growth *in vitro* and *in vivo*. **A,** Negative-selection competition assay showing the percentage of GFP^+ empty vector (ev) or sgKAT6A-transduced cells over time, normalized to day 3 ($n = 2$–3 each group). **B,** Cell-cycle analysis after 7 days of ev or sgKAT6A-2 transduction in MOLM-13 cells ($n = 4$ each group). **C,** Count of colonies formed by 2,000 or 1,000 MOLM-13 cells after ev or sgKAT6A-2 transduction ($n = 6$ each group). **D,** Senescence-associated β-galactosidase activity in MOLM-13 cells measured by flow cytometry ($n = 4$ each group). MFI, mean fluorescence intensity. **E,** Quantification of bioluminescence of mice transplanted with ev or sgKAT6A MOLM-13-luc cells over time, normalized to day 2 ($n = 7$ each group). **F,** Bioluminescent images of mice transplanted with ev or sgKAT6A MOLM-13-luc cells on day 16 ($n = 7$ each group). **G,** Kaplan–Meier survival plot of mice transplanted with ev or sgKAT6A MOLM-13-luc cells ($n = 7$ each group). **H,** Negative-selection competition assay showing the percentage of $mCherry^+$ ev or sgKat6a-transduced cells over time, normalized to day 6 ($n = 2$ each group). **I,** Count of colonies formed by 1,000 mouse MLL–AF9 cells after ev or sgKat6a-6 transduction ($n = 6$ each group). **J,** Leukemia burden quantified by the ratio of GFP^+ mouse MLL–AF9 cells in the bone marrow of mice three weeks after transplantation ($n = 5$ each group). **K,** Negative-selection competition assay in MOLM-13 cells showing the percentage of GFP^+ ev or sgKAT6A-transduced cells normalized to day 6, following overexpression of indicated *KAT6A* cDNA constructs. Statistical differences were calculated using two-way ANOVA with multiple comparisons (**A** and **E**), multiple *t* test (**B** and **C**), unpaired Student *t* test (**D**, **I**, and **J**), and log-rank test (**G**). Error bars in **E**, mean ± SEM; error bars in all other panels, mean ± SD; $P < 0.05$ was considered statistically significant; *, $P < 0.05$; **, $P < 0.01$; ***, $P < 0.001$. See also Supplementary Fig. S2.

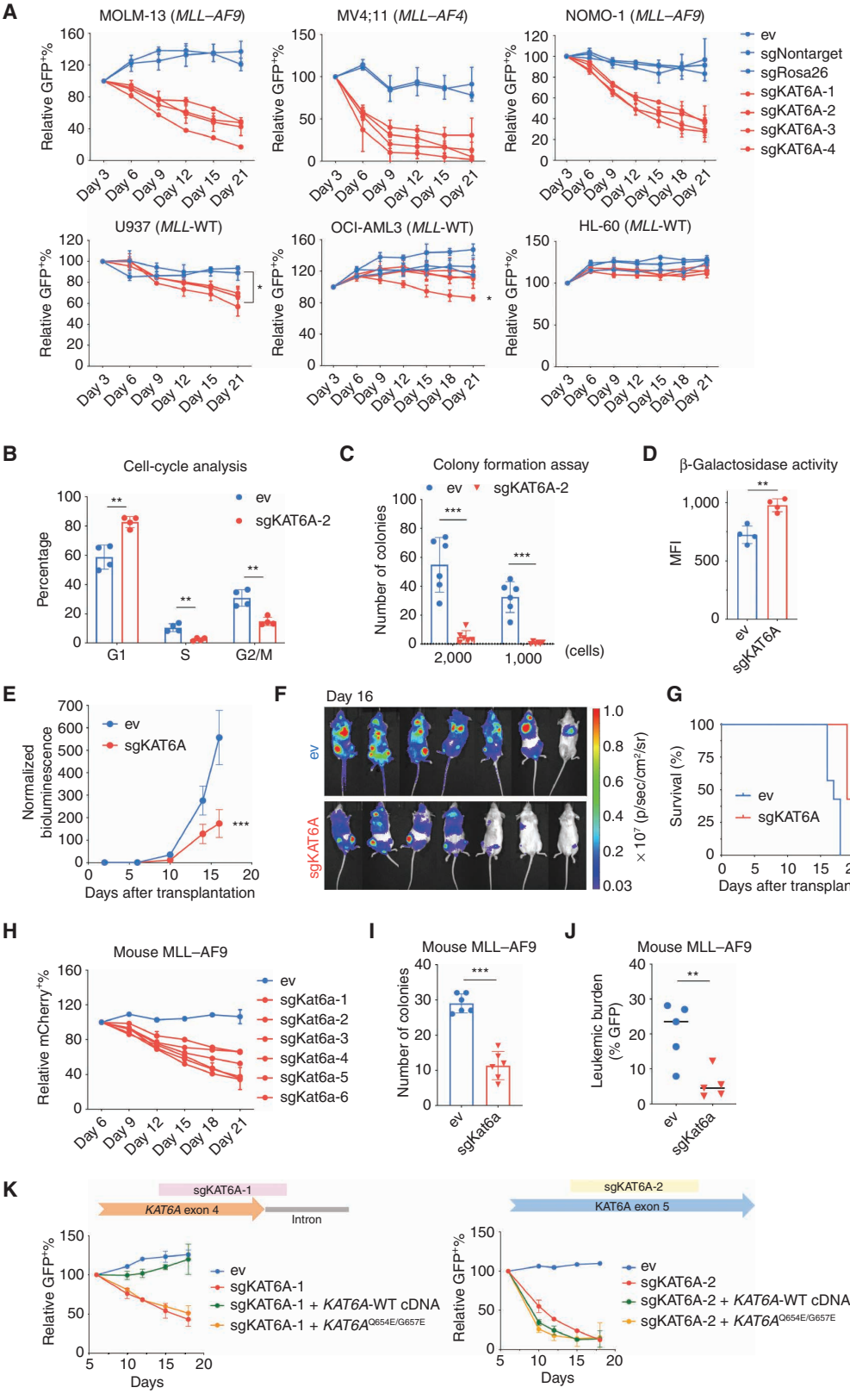

or both. To test the importance of KAT6A catalytic activity, we attempted to rescue the sgKAT6A proliferation phenotype with cDNA expression of WT *KAT6A* or catalytic dead *KAT6A*$^{Q654E/G657E}$, in which the Q654E and G657E point mutations completely abrogate KAT6A acetyltransferase activity (50). We found that WT *KAT6A*, but not mutant *KAT6A*$^{Q654E/G657E}$, fully rescued the growth defect of cells expressing a *KAT6A* sgRNA that only targeted endogenous protein by spanning an exon–intron junction (Fig. 2K; Supplementary Fig. S2F). As expected, neither WT nor mutant *KAT6A* rescued the phenotype of a *KAT6A* sgRNA that targeted both the endogenous and exogenous proteins. These results demonstrate that acetyltransferase activity is essential for KAT6A to maintain AML growth.

Loss of KAT6A Disrupts MYC-Related Transcriptional Programs

We sought to understand the molecular mechanism underlying KAT6A-controlled AML growth and differentiation. Given the importance of KAT6A acetyltransferase activity and the role of histone acetylation in gene activation, we hypothesized that KAT6A might be driving AML oncogene expression via histone acetylation.

To identify potential transcriptional targets of KAT6A, we performed RNA-seq of *KAT6A*-WT versus *KAT6A*-KO MOLM-13 cells (Supplementary Fig. S3A). Among the significantly downregulated genes following KAT6A depletion, we found several of the most critical drivers of leukemogenesis, including *MYC*, *MYB*, and *FLT3*, as well as other more recently identified genes of interest such as the MLL-fusion target gene *LAMP5* (ref. 51; Fig. 3A). Consistent with the induction of myeloid differentiation (Fig. 1G), we also observed upregulation of *ITGAM* (encoding CD11b), *CSF1R*, and *CD86*. On the pathway level, gene set enrichment analysis (GSEA) revealed a gain of myeloid differentiation–related signatures (46, 52) and loss of the leukemia stem cell (LSC) signature (53) upon *KAT6A* KO (Fig. 3B; Supplementary Fig. S3B). In line with the observed growth defects, the most dramatically downregulated gene sets included cell-cycle–related gene signatures and MYC target genes, with the most repressed signature overall being the combined hallmark MYC target gene set [normalized enrichment score (NES) = –3.718; Fig. 3C; Supplementary Fig. S3C]. Finally, motif analysis predicted enrichment of MYC and E2F DNA binding motifs in promoters of those downregulated genes, whereas motifs of hematopoietic transcription factors PU.1 and IRF8 were enriched in upregulated gene promoters, consistent with myeloid lineage maturation (Fig. 3D; Supplementary Fig. S3D).

As our RNA-seq data suggest that KAT6A may help drive a critical MYC-focused transcriptional program, we aimed to further confirm KAT6A-mediated activation of *MYC* with orthogonal methods. First, we inhibited *KAT6A* via shRNA knockdown in several cell lines and observed *MYC* downregulation in all cases, including in non–MLL-r U937 cells, indicating that *MYC* regulation by KAT6A is not due to sgRNA off-target effects and is not limited to MOLM-13 cells (Supplementary Fig. S3E and S3F). Western blot also showed MYC downregulation on protein level following KAT6A depletion (Supplementary Fig. S3G). Overexpression of *MYC* in *KAT6A*-KO cells partially rescued the growth phenotype (Supplementary Fig. S3H). We then tested whether exogenous overexpression of *KAT6A* would further upregulate *MYC*. Indeed, we found that overexpression of WT *KAT6A*, but not catalytic dead *KAT6A*$^{Q654E/G657E}$, increased *MYC* expression (Fig. 3E).

Consistent with the results in human cell lines, in mouse MLL–AF9 cells, *Kat6a* KO also resulted in downregulation in *Myc* expression (Supplementary Fig. S3I).

Given that MYC is a master transcription factor in promoting leukemogenesis, these results suggest that *MYC* activation may represent a key mechanism by which KAT6A sustains oncogenic gene-expression programs in AML.

KAT6A Regulates H3K9ac on Key Leukemogenic Genes

KAT6A can catalyze H3K9ac, H3K14ac, and H3K23ac (38). We wondered which, if any, of these histone acetylation modifications are involved in KAT6A-regulated leukemogenic gene expression. Western blots showed a modest global reduction of H3K9ac upon KAT6A depletion, but no apparent changes in H3K14ac and H3K23ac (Fig. 4A; Supplementary Fig. S4A). To investigate locus-specific histone acetylation dynamics, we performed chromatin immunoprecipitation sequencing (ChIP-seq) of each of these histone modifications in WT and *KAT6A*-KO MOLM-13 cells (Supplementary Fig. S4B and S4C; Supplementary Table S3). We also performed HA-KAT6A ChIP-seq in WT cells to identify KAT6A direct binding sites (Supplementary Table S4). We found that HA-KAT6A binding is extremely specific (>90% of peaks) to promoters (Fig. 4B), and highly overlapping with H3K9ac, H3K14ac, and H3K23ac peaks (Fig. 4C). However, although co-occurrence of HA-KAT6A and these three modifications was common, the enrichment magnitude of H3K9ac at HA-KAT6A binding sites was far stronger than that of H3K14ac or H3K23ac (Fig. 4C). Notably, H3K9ac was also the most responsive to *KAT6A* KO at HA-KAT6A binding sites (Fig. 4D). Two hundred forty-five H3K9ac peaks that overlapped HA-KAT6A peaks were decreased upon *KAT6A* KO, and only six were increased. In contrast, fewer than 20 such H3K14ac or H3K23ac peaks were changed upon KAT6A depletion (Fig. 4D). Furthermore, HA-KAT6A was highly enriched at genomic loci that lost H3K9ac following depletion of KAT6A, but showed no enrichment at regions where H3K9ac increased (Supplementary Fig. S4D).

We next investigated the relation between acetylation dynamics and transcription. Upon KAT6A depletion, we found that loss or gain of H3K9ac—but not H3K14ac or H3K23ac—was strongly associated with transcriptional downregulation or upregulation, respectively (Fig. 4E; Supplementary Fig. S4E). We then identified gene pathways (54) and transcription factor binding motifs associated with H3K9ac dynamics. Cell-cycle regulators and MYC activity, as well as E2F and MYC motifs, were enriched in genes losing H3K9ac in response to *KAT6A* KO. Genes gaining H3K9ac also showed dramatic enrichment of myeloid differentiation signatures and related TF motifs, such as PU.1, IRF8, and several ETS factors (Supplementary Fig. S4F and S4G), consistent with transcriptional changes following KAT6A deletion. Together, these findings strongly implicate H3K9ac, rather than H3K14ac or H3K23ac, as the key catalytic target

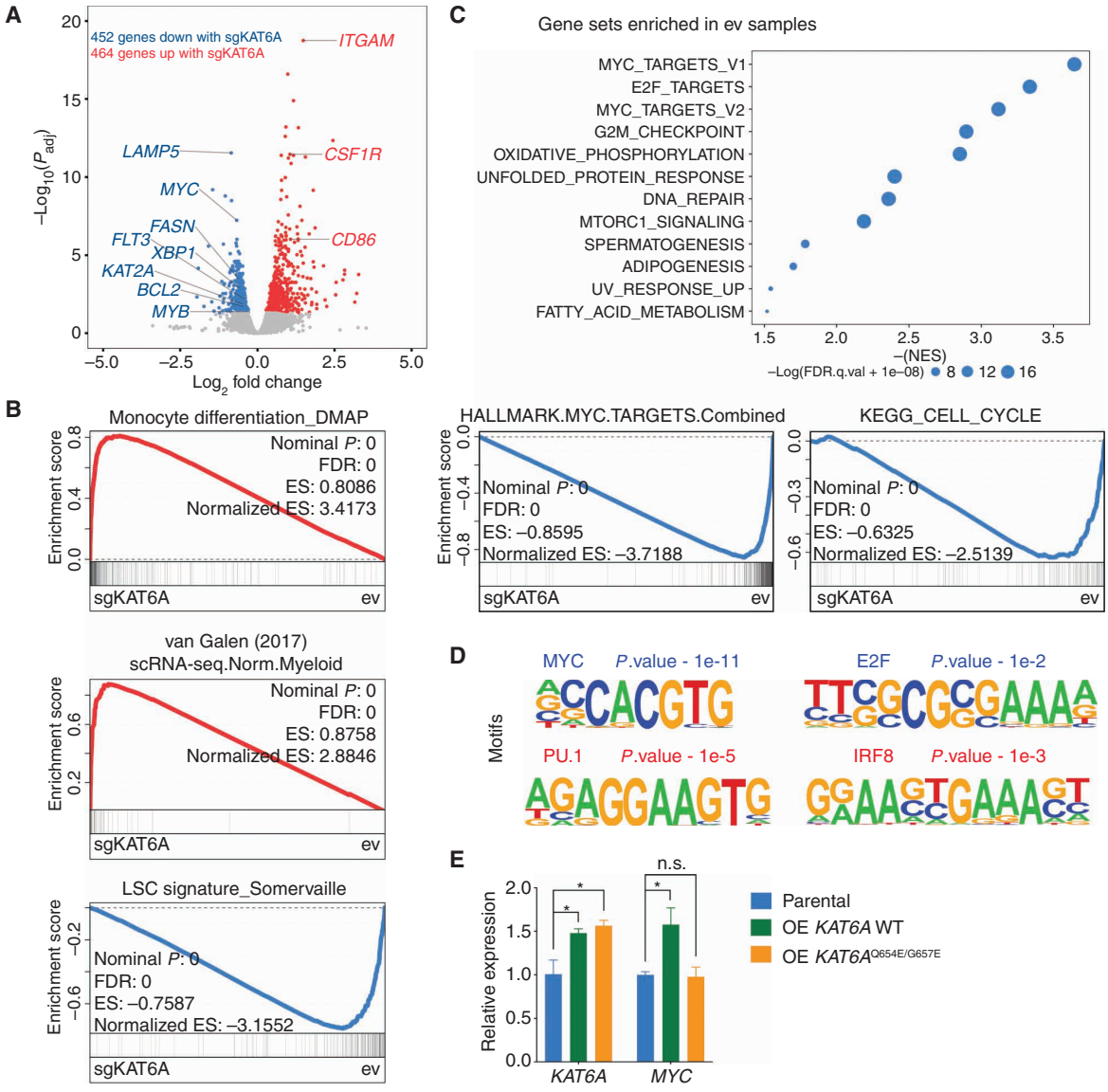

Figure 3. Loss of KAT6A disrupts MYC-related transcriptional programs. **A,** Volcano plot showing the differentially expressed genes between empty vector (ev) and sgKAT6A-2–transduced MOLM-13 cells five days after viral transduction. Genes with $P_{adj} < 0.05$ are highlighted (blue: genes downregulated in sgKAT6A cells; red: genes upregulated in sgKAT6A cells). **B,** Leading-edge plots showing the enrichment of indicated gene sets based on GSEA (blue: gene set enriched in ev cells; red: gene set enriched in sgKAT6A cells). ES, enrichment score; FDR, false discovery rate; scRNA-seq, single-cell RNA-seq. **C,** Top enriched hallmark gene sets in ev cells based on GSEA (top). Representative leading-edge plots of the combined hallmark MYC target (V1 + V2) gene set (bottom left) and Kyoto Encyclopedia of Genes and Genomes (KEGG) cell-cycle gene set (bottom right). **D,** Top transcription factor motifs enriched in transcription start site regions (−1 kb to +300 bp) of sgKAT6A-downregulated genes (blue) and sgKAT6A-upregulated genes (red). **E,** mRNA expression of *KAT6A* and *MYC* in parental MOLM-13 cells or with indicated constructs. OE, overexpression. Statistical differences were calculated using one-way ANOVA with multiple comparisons (**E**). All error bars represent mean ± SD, and $P < 0.05$ was considered statistically significant; *, $P < 0.05$; n.s., not significant. See also Supplementary Fig. S3.

of KAT6A in its role as a driver of stemness and proliferation gene-expression programs in AML.

To define the potential KAT6A direct target genes, we focused on 28 genes that met all three criteria: HA-KAT6A direct binding, loss of H3K9ac upon KAT6A depletion, and transcriptional downregulation upon KAT6A depletion (Fig. 4F). This "core KAT6A target gene set" was markedly enriched for key leukemogenic genes, including *MYC*, *MYB*, and *LAMP5* (Fig. 4F). Additional manual inspection uncovered strong trends in other key KAT6A targets not initially identified in this core gene set, such as *HOXA9* and *MEIS1*. We further confirmed through qPCR that KAT6A regulates these genes as well (Supplementary Fig. S4H). Notably, H3K9ac reductions were almost exclusively observed at promoters of these KAT6A

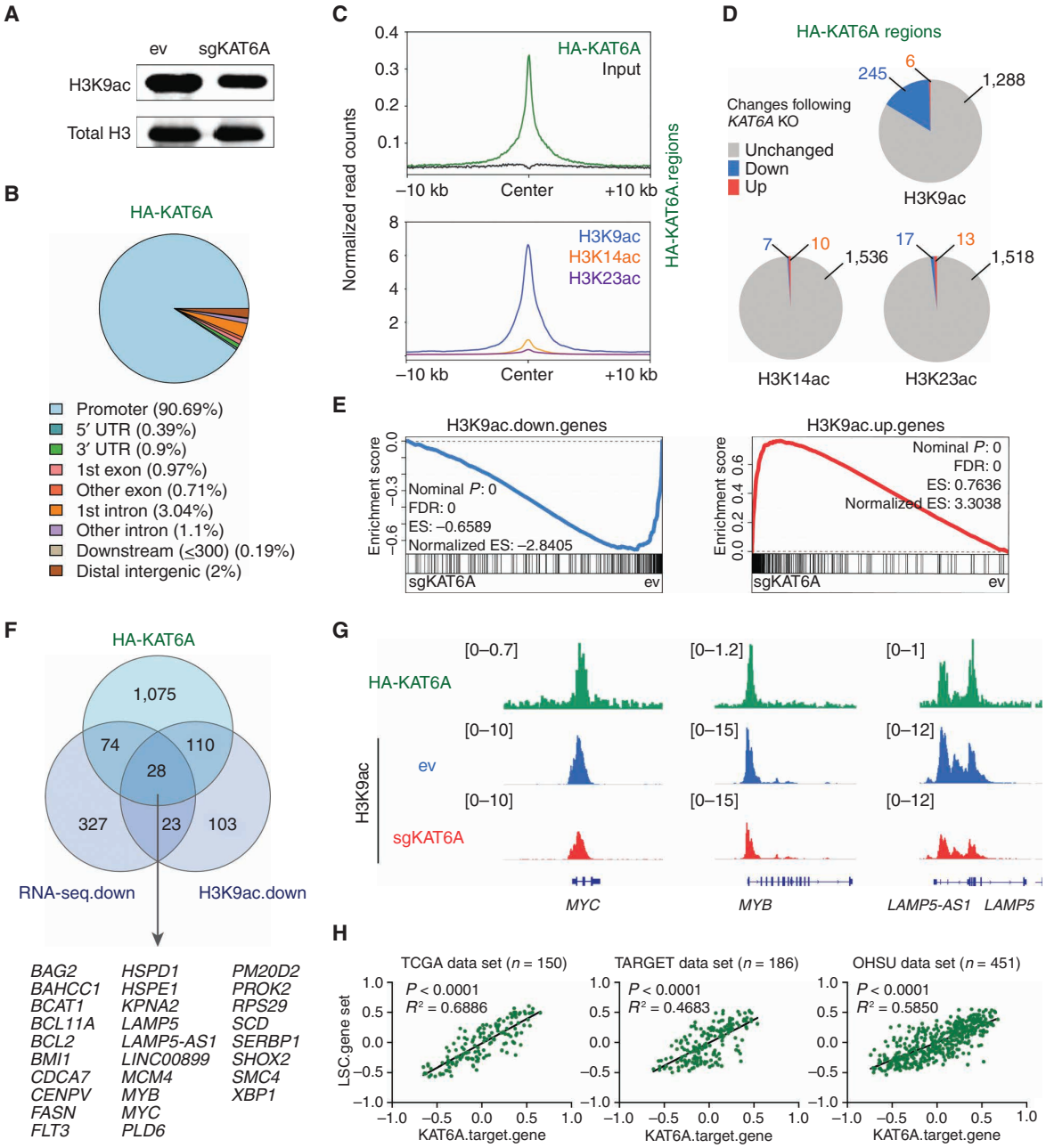

Figure 4. KAT6A regulates H3K9ac on key leukemogenic genes. **A,** Western blot of H3K9ac and total H3 in empty vector (ev) and sgKAT6A-2–transduced MOLM-13 cells five days after viral transduction. UTR, untranslated region. **B,** Pie chart showing genomic annotations of HA-KAT6A ChIP-seq peaks. **C,** Distribution of normalized ChIP-seq reads for HA-KAT6A (top) and indicated histone marks (bottom) centered on HA-KAT6A peaks. **D,** Pie charts showing changes ($P < 0.05$) of histone acetylation marks at genomic regions where HA-KAT6A intersects with histone acetylation marks. **E,** Leading-edge plots showing the enrichment of genes associated with H3K9ac downregulated or upregulated regions based on GSEA of ev and sgKAT6A samples. ES, enrichment score; FDR, false discovery rate. **F,** Venn diagram showing the overlap of HA-KAT6A–bound genes, genes downregulated with sgKAT6A ($P_{adj} < 0.05$), and genes associated with H3K9ac downregulated regions ($P < 0.05$). **G,** Genome tracks showing HA-KAT6A and H3K9ac ChIP-seq occupancy at indicated gene loci. **H,** Pearson correlation of sample-wise KAT6A target gene set enrichment scores and LSC gene set enrichment scores calculated by gene set variation analysis. Each dot represents one sample from TCGA, TARGET, or OHSU data sets. See also Supplementary Fig. S4.

target genes rather than distal regulatory elements (Fig. 4G; Supplementary Fig. S4C; Supplementary Fig. S4I). We then explored the relevance of this core gene set to AML in the clinical context, and we found a remarkably strong correlation between expression levels of KAT6A target genes and LSC genes (53) in TCGA, TARGET, and Oregon Health & Science University (OHSU; ref. 55) patients (Fig. 4H). Importantly, the core KAT6A target gene set and LSC gene set have only two overlapping genes (Supplementary Fig. S4J), indicating that this correlation is not due to the presence of shared genes, but is indeed a real interrelationship between two independent gene sets. Finally, we also found that KAT6A target gene levels are inversely correlated with cell differentiation status in a genetically defined, doxycycline-induced AML differentiation model (ref. 56; Supplementary Fig. S4K).

Collectively, these data suggest that KAT6A drives expression of a core oncogenic program through maintaining promoter H3K9ac.

The H3K9ac Reader ENL Is a Downstream Effector of KAT6A

To further understand the function of KAT6A in AML, we explored the Cancer Dependency Map (DepMap; refs. 57, 58), a database of results from genome-wide CRISPR–Cas9 and RNAi dropout (proliferation/survival) screens performed in hundreds of cancer cell lines. We queried *KAT6A* codependencies, which are genes with a high correlation to *KAT6A* in degree of essentiality (i.e., dropout scores) across all cell lines. High codependency is suggestive of common functionality, such as membership in the same protein complex or signaling pathway. Encouragingly, the top *KAT6A* codependency in the CRISPR screen database was *BRPF1*, which encodes the core structural component of the KAT6A complex. *KAT6B*, a homolog of *KAT6A*, was also among the top *KAT6A* codependent genes (Fig. 5A). Intriguingly, among the top *KAT6A* codependencies in both the CRISPR and RNAi screen databases, we found *MLLT1* (*ENL*; Fig. 5A; Supplementary Fig. S5A), a protein that binds H3K9ac, H3K27ac, and other histone acyl modifications and is essential in maintaining oncogenic gene expression in AML (25, 26). As ENL "reads" H3K9ac and sustains *MYC* expression in leukemia cells, this finding implicates the possibility of a "writer–reader" module in which KAT6A provides the H3K9ac that is bound by ENL to promote transcription at oncogene promoters.

If KAT6A and ENL function cooperatively in AML, we would expect them to regulate similar genes and colocalize at key oncogenic loci. To test this hypothesis, we integrated our RNA-seq and ChIP-seq data with published ENL epigenomic data sets, as MOLM-13 cells were used in both cases. We first interrogated RNA-seq data and found that loss of ENL and KAT6A induced highly concordant transcriptional changes (Fig. 5B). We then investigated chromatin occupancy and found that HA-KAT6A, FLAG-ENL, and H3K9ac are all strongly colocalized on chromatin (Fig. 5C). In fact, nearly half (567/1,334) of the FLAG-ENL peaks are overlapping with HA-KAT6A–localized genomic regions, representing a remarkable degree of "writer–reader" colocalization (Supplementary Tables S4–S6). It is possible that, as an H3K9ac reader, ENL may colocalize with any set of H3K9ac peaks. To determine if ENL binding is specific to KAT6A-regulated H3K9ac, we analyzed FLAG-ENL binding at H3K9ac loci that either decreased after *KAT6A* KO (i.e., KAT6A-regulated H3K9ac) or increased/unchanged after *KAT6A* KO (i.e., non–KAT6A-regulated H3K9ac). We found that FLAG-ENL was highly enriched at loci that lost H3K9ac upon KAT6A depletion but showed no enrichment at regions where H3K9ac were increased/unchanged after KO (Fig. 5D). This suggests that ENL preferentially binds the subset of H3K9ac that is regulated by KAT6A.

We next tested whether ENL is dependent on KAT6A-catalyzed H3K9ac for chromatin binding. In accordance with our model, ChIP-seq revealed strong global loss of H3K9ac and ENL at KAT6A-binding sites following KAT6A depletion (Supplementary Fig. S5B). Besides global changes, we then used ChIP-qPCR to confirm our findings at key target genes *MYC* and *MYB*, and found marked reduction of ENL at both genes in *KAT6A*-KO cells (Fig. 5E). These results suggest that ENL is evicted from chromatin upon loss of KAT6A-catalyzed H3K9ac.

ENL recruits transcriptional machinery to chromatin, and previous work (25) showed that loss of ENL reduces local RNA Pol II chromatin binding. We investigated whether KAT6A-regulated H3K9ac may initiate this program. We integrated Pol II ChIP-seq data from sgENL (*ENL* KO) and sgGFP (*ENL* WT) MOLM-13 cells into our H3K9ac ChIP-seq data sets. We found that ENL depletion led to reduced Pol II binding at KAT6A-binding sites (Supplementary Fig. S5B). Intriguingly, reduction of Pol II binding occurred only at KAT6A-regulated H3K9ac regions, but other H3K9ac loci are minimally affected (Fig. 5F). These results suggest a model in which KAT6A catalyzes promoter H3K9ac that is bound by ENL, which subsequently recruits Pol II to sustain AML oncogene expression and block differentiation.

Accordingly, we propose a "KAT6A–ENL–Pol II" axis that highlights the role of promoter H3K9ac in AML transcriptional control.

KAT6A Influences a Network of MLL-r AML-Related Chromatin and Transcription Regulators

Several lines of evidence suggest that a broader network of MLL-r AML-related transcriptional regulators may be ultimately dependent on KAT6A and its catalysis of H3K9ac. First, ENL, proposed here as downstream of KAT6A, recruits multiple MLL-r AML-related chromatin factors to oncogenic loci, such as CDK9 and DOT1L-catalyzed H3K79me2 and H3K79me3 (25, 26, 59). Second, several MLL-r AML-related factors were also found among the top five *KAT6A* codependencies in the DepMap, including *KMT2A* (*MLL1*), *DOT1L*, and *ASH1L* (36, 60; Supplementary Fig. S5C). Finally, as shown earlier, MLL-r AMLs are more dependent on KAT6A than on MLL-WT AMLs (Fig. 2A; Supplementary Fig. S2A).

To investigate whether KAT6A may help orchestrate this MLL-r transcriptional control network, we tested whether the ENL-recruited factors CDK9, H3K79me2, and H3K79me3 colocalize with KAT6A-regulated H3K9ac. Indeed, all three were strongly enriched at KAT6A-regulated H3K9ac loci but had minimal binding at nonregulated H3K9ac loci (Supplementary Fig. S5D). Further, as with Pol II, ENL depletion reduced the binding of these factors only at these KAT6A-regulated H3K9ac loci, not at nontarget H3K9ac (Supplementary Fig. S5D).

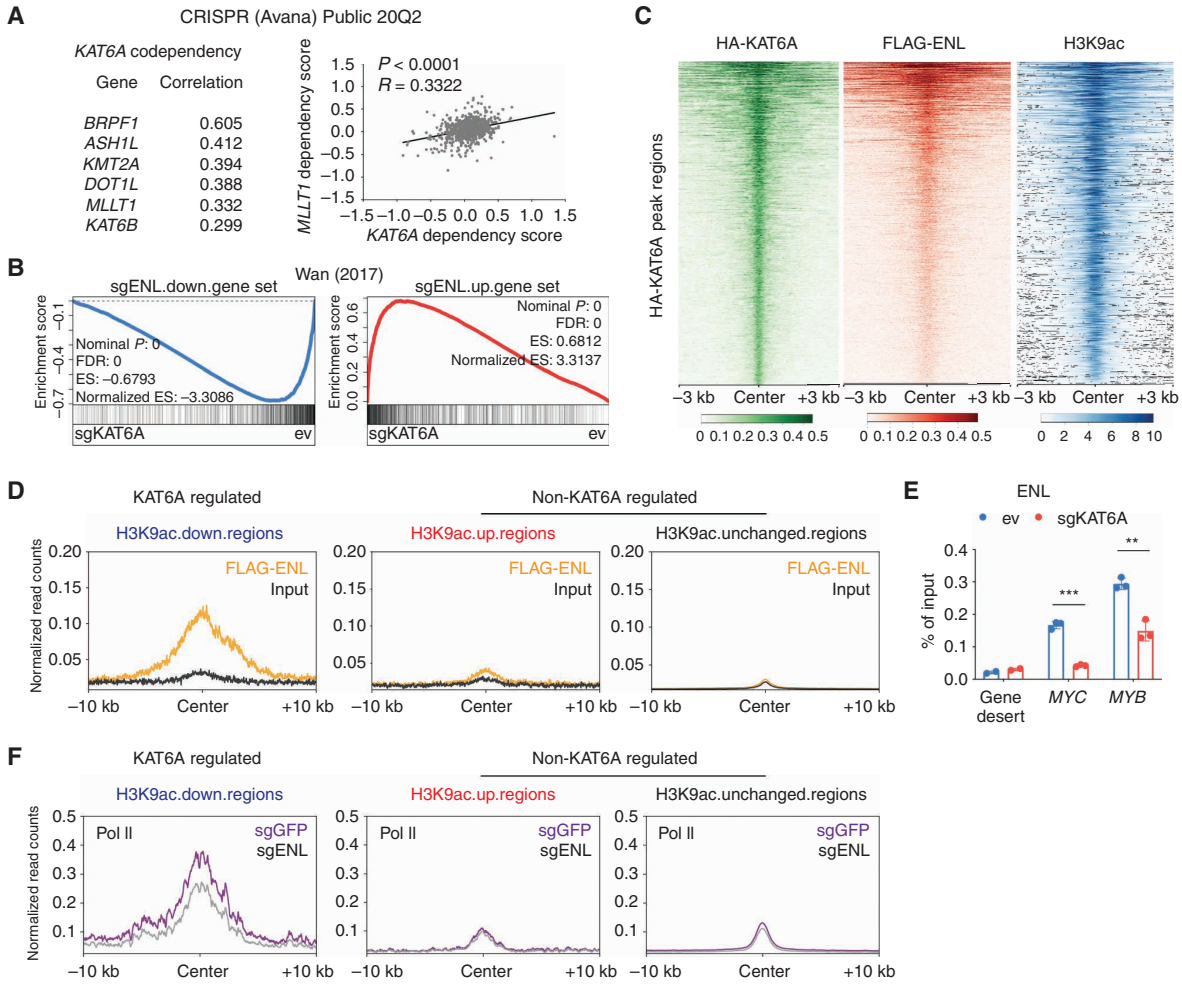

Figure 5. The H3K9ac reader ENL is a downstream effector of KAT6A. **A,** DepMap CRISPR Public 20Q2 data set showing the top codependent genes with *KAT6A* and their Pearson correlation scores (left). Correlation of *KAT6A* and *MLLT1* (*ENL*) dependency scores is presented (right). Each dot represents a cell line. **B,** Leading-edge plots showing the enrichment of genes downregulated or upregulated by sgENL in MOLM-13 cells (data from GSE80774) based on GSEA of empty vector (ev) and sgKAT6A samples. ES, enrichment score; FDR, false discovery rate. **C,** Heat maps showing ChIP-seq signals of HA-KAT6A, FLAG-ENL (data from GSE80779), and H3K9ac centered on HA-KAT6A peaks in MOLM-13 cells. **D,** Distribution of normalized ChIP-seq reads for FLAG-ENL in MOLM-13 cells (data from GSE80779) centered on H3K9ac downregulated, upregulated, or unchanged regions. **E,** ChIP-qPCR of ENL at gene desert as well as *MYC* [transcription start site (TSS) + 1 kb] and *MYB* (TSS + 2 kb) loci after five days of ev and sgKAT6A-2 transduction in MOLM-13 cells. **F,** Distribution of normalized ChIP-seq reads for RNA Pol II with sgGFP or sgENL in MOLM-13 cells (data from GSE80779) centered on H3K9ac downregulated, upregulated, or unchanged regions. Statistical differences were calculated using multiple *t* test (**E**). All error bars represent mean ± SD, and $P < 0.05$ was considered statistically significant; **, $P < 0.01$; ***, $P < 0.001$. See also Supplementary Fig. S5.

To ensure our findings were not unique to our integration of the data set from Wan and colleagues, we performed similar analyses using data from an independent study (61). We integrated our data with ChIP-seq and RNA-seq data related to MLL1/MLL-AF9, Menin, DOT1L, and DOT1L-catalyzed H3K79me2 in MOLM-13 cells. In accordance with previous results, we found that all four factors were strongly colocalized at KAT6A-regulated H3K9ac regions, but not at nonregulated H3K9ac loci (Supplementary Fig. S5E). We then analyzed RNA-seq data from VTP50469, which inhibits the Menin–MLL interaction, and the DOT1L inhibitor EPZ-5676 in MOLM-13 cells (Supplementary Table S7). Consistent with our model, both inhibitors induce transcriptional changes that are highly similar to those resulting from KAT6A depletion (Supplementary Fig. S5F).

Finally, we asked whether our model of KAT6A/H3K9ac-based transcriptional control was supported in clinical AML samples. A key feature of our model is the convergence of KAT6A, ENL, and other MLL-r AML-related factors in the regulation of AML oncogenic programs. To test whether these factors may operate in unison in clinical AML, we clustered patients of the TCGA, TARGET, and OHSU data sets according to their enrichment of the LSC signature, monocyte differentiation signature, and differential gene-expression

signatures from *KAT6A*-KO, *ENL*-KO, EPZ-5676 (DOT1L inhibitor), and VTP50469 (Menin inhibitor) treatment. In accordance with predictions, enrichment scores of all four gene inhibition signatures correlated strongly with one another. Further, enrichment of the monocyte maturation signature correlated with inhibition of all four genes, whereas enrichment of the LSC signature correlated with activation of all four genes (Supplementary Fig. S5G).

Taken together, these data are consistent with a model in which the KAT6A–ENL histone acetylation write–read module cooperates with MLL-r–related chromatin factors to drive leukemogenic gene-expression programs.

WM-1119 Treatment Inhibits the KAT6A-Mediated Transcriptional Program and AML Growth

Our findings suggest that KAT6A may represent a novel target of interest for prodifferentiation therapeutics in non-APL AML. Although previously considered "undruggable," breakthrough work recently provided the first-in-class KAT6A/B inhibitor WM-8014 and its derivative WM-1119 (48). These inhibitors render us the opportunity to explore their efficacy in AML models. As *in vivo* use of these inhibitors is challenging, we focused on surrogate *in vitro* assays for proof of principle.

To determine whether the inhibitors yield similar results as genetic KO of *KAT6A*, we tested their effects on differentiation, proliferation, and clonogenic potential. In addition to using human AML cell lines, we tested responses in primary cells from several genetically defined mouse MLL–AF9 models, to ensure our results are not unique to cell culture–adapted cell lines. In virtually all assays, inhibitor responses phenocopied results from genetic inhibition of KAT6A. Treatment of inhibitors significantly or near significantly increased CD11b in all cells assayed, and reduced EdU positivity in the MLL–AF9 models MOLM-13, MV4;11, and RN2 (*MLL–AF9/NRas*^{G12D}; ref. 62). Additionally, WM-1119 treatment impaired colony formation ability in MOLM-13, MV4;11, and NOMO-1 cells, and almost fully abolished it in RN2 and the MLL-r-like ER–HOXA9 and ER–HOXB8 (63, 64) primary mouse cell models (Fig. 6A–C; Supplementary Fig. S6A–S6C). Similar to genetic KO, WM-1119 treatment also induced superoxide anion production (functional differentiation) and β-galactosidase activity (senescence) in MOLM-13 cells (Supplementary Fig. S6D and S6E).

Transcriptional changes mediated by WM-1119 were also determined in human MOLM-13 and mouse ER–HOXA9 cells. The responses again phenocopied those of *KAT6A*-KO cells, in which marked downregulation of *MYC/Myc* and LSC signatures was observed (Fig. 6D–G; Supplementary Fig. S6F–S6H). Interestingly, although ChIP-seq of WM-1119–treated cells revealed locus-specific H3K9ac loss on leukemogenic genes similar to *KAT6A* KO (Fig. 6H–J), global levels of H3K9ac remained mostly unchanged (Supplementary Fig. S6I and S6J). Rather, histone mass spectrometry of MOLM-13 cells treated with WM-1119 revealed dramatic loss of H3K23ac (Supplementary Fig. S6I), which is likely due to the effect of cotargeting KAT6B (65, 66).

Finally, we tested the combinatorial efficacy of WM-1119 and other anti-AML agents already in clinical trials, including SAHA (histone deacetylase inhibitor; ref. 67), EPZ-5676 (DOT1L inhibitor; ref. 68), 5-Aza (69), decitabine (DNA methylation inhibitor; ref. 70), SNDX-5613 (Menin–MLL inhibitor, ongoing trial NCT04065399), and ORY-1001 (LSD1 inhibitor, ongoing trial EudraCT 2018-000482-36). Using surface CD11b level as a readout, we found that drug responses were potentiated by WM-1119 and that combination with ORY-1001 appeared the most potent (Supplementary Fig. S6K). Cell viability assessment showed a stronger synergy between WM-1119 and ORY-1001/EPZ-5676/SNDX-5613 (Supplementary Fig. S6L). We confirmed the efficacy of the WM-1119/ORY-1001 combination in colony formation assays, in which self-renewal was depleted synergistically by inhibitor cotreatment (Supplementary Fig. S6M).

The clinical relevance of the WM-1119 inhibitor was also evaluated by *ex vivo* culturing of primary human AML cells. In the colony formation assays of the primary cells, patient samples with MLL-r subtype AML (AML-010 and AML-6457) were sensitive to WM-1119 treatment, and the response was further potentiated by ORY-1001/EPZ-5676 treatment. On the contrary, patient samples with MLL-WT AML (AML-7050 and AML-7052) were insensitive to WM-1119 treatment (Fig. 6K). This is consistent with the drug sensitivity observed in AML cell lines (Supplementary Fig. S6N). On a molecular level, we confirmed that WM-1119 reduced *MYC* expression and H3K9ac levels in MLL-r primary AML samples (Fig. 6L; Supplementary Fig. S6O).

Together, these results suggest that the KAT6A inhibitor, alone or in combination with other inhibitors, represents a promising therapeutic strategy for treatment of AML.

DISCUSSION

AMLs are described as being "addicted" to selected oncogenic transcription programs, and these programs require support from chromatin regulators to maintain their hyperactive state (71). Accordingly, epigenetic dysregulation is a hallmark characteristic of AML, and mutations in epigenetic regulators are dramatically overrepresented in the AML genome (42). However, the co-opting of WT proteins to support aberrant transcriptional programs has been increasingly appreciated only in recent years. Identification of such chromatin regulators is of high interest, as they typically represent more attractive therapeutic targets than their associated transcription factors.

The KAT6A (MOZ) translocation MOZ–TIF2 has been long known as a rare driver event in AML (72), but a function for WT KAT6A in leukemia differentiation has not been previously reported. Here, we found that WT KAT6A is a novel dependency in AML that drives oncogene expression by regulating promoter H3K9ac levels. Notably, several other MYST HATs have been shown to promote AML oncogenesis. Most recently, HBO1/KAT7 was shown to support LSC activity through acetylation of H3K14 at target genes, promoting elevated transcriptional elongation of key oncogenes such as *Hoxa9* (73). MOF/KAT8 was also implicated in MLL-r AML, in which its catalysis of H4K16ac was shown to drive expression of genes involved in DNA damage repair (74). These and related reports suggest that multiple HATs are required for AML oncogenesis, but may play diverse and distinct roles in transcriptional regulation.

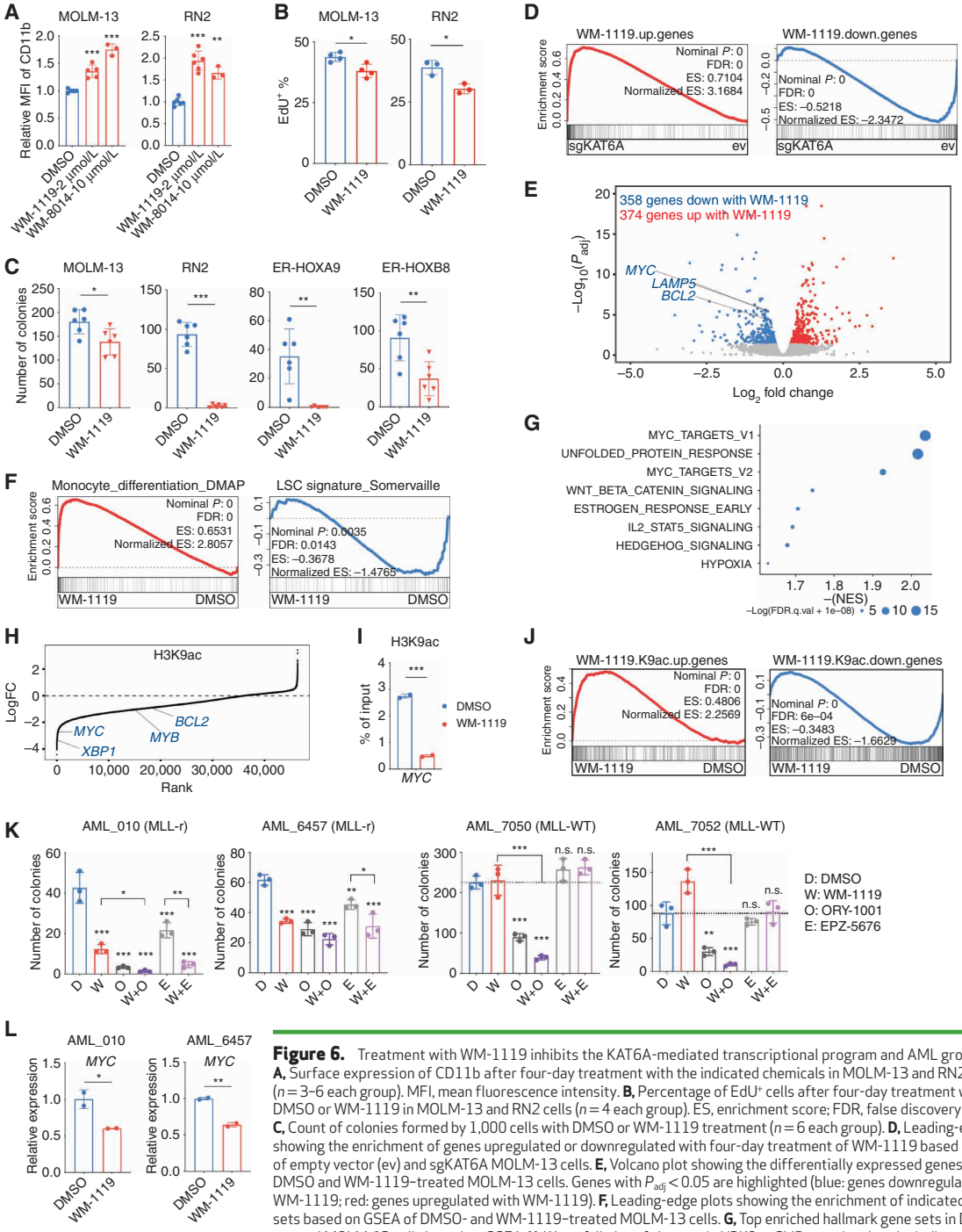

Figure 6. Treatment with WM-1119 inhibits the KAT6A-mediated transcriptional program and AML growth. **A,** Surface expression of CD11b after four-day treatment with the indicated chemicals in MOLM-13 and RN2 cells ($n = 3$–6 each group). MFI, mean fluorescence intensity. **B,** Percentage of EdU$^+$ cells after four-day treatment with DMSO or WM-1119 in MOLM-13 and RN2 cells ($n = 4$ each group). ES, enrichment score; FDR, false discovery rate. **C,** Count of colonies formed by 1,000 cells with DMSO or WM-1119 treatment ($n = 6$ each group). **D,** Leading-edge plots showing the enrichment of genes upregulated or downregulated with four-day treatment of WM-1119 based on GSEA of empty vector (ev) and sgKAT6A MOLM-13 cells. **E,** Volcano plot showing the differentially expressed genes between DMSO and WM-1119–treated MOLM-13 cells. Genes with $P_{adj} < 0.05$ are highlighted (blue: genes downregulated with WM-1119; red: genes upregulated with WM-1119). **F,** Leading-edge plots showing the enrichment of indicated gene sets based on GSEA of DMSO- and WM-1119–treated MOLM-13 cells. **G,** Top enriched hallmark gene sets in DMSO-treated MOLM-13 cells based on GSEA. **H,** Waterfall plot of changes in H3K9ac ChIP-seq signal at the indicated proximal genes after four days of WM-1119 treatment in MOLM-13 cells. logFC, log fold change. **I,** ChIP-qPCR of H3K9ac at a gene desert or the *MYC* locus after four-day treatment with DMSO or WM-1119 in MOLM-13 cells. **J,** Leading-edge plots showing the enrichment of genes associated with H3K9ac upregulated or downregulated regions following WM-1119 treatment, based on GSEA of RNA-seq data from DMSO- and WM-1119–treated MOLM-13 cells. **K,** Count of colonies formed by primary human AML cells after indicated chemical treatment ($n = 3$ technical replicates/group). WM-1119: 10 μmol/L; ORY-1001: 25 nmol/L; EPZ-5676: 50 nmol/L. **L,** mRNA expression of *MYC* after three days of WM-1119 treatment in primary human AML cells. Statistical differences were calculated using one-way ANOVA with multiple comparisons (**A** and **K**) and an unpaired Student *t* test (**B**, **C**, **I**, and **L**). All error bars represent mean ± SD, and $P < 0.05$ was considered statistically significant; *, $P < 0.05$; **, $P < 0.01$; ***, $P < 0.001$; n.s., not significant. Treatment was carried out with 4 μmol/L WM-1119, if not otherwise indicated. See also Supplementary Fig. S6.

Recent work (25, 26) identified the H3K9ac and H3K27ac binding functionality of the YEATS domain protein ENL and uncovered the importance of H3K9ac "reading" by ENL at promoters of AML oncogenes such as *MYC*. However, the writer responsible for H3K9ac in this context remained unknown. Here, we propose that KAT6A is the key H3K9 acetyltransferase that provides substrate for ENL binding in AML. As ENL recruits transcriptional activation and elongation machinery, KAT6A and ENL appear to function in tandem as a writer–reader "module" dedicated to facilitating the later stages of transcriptional activation of *MYC*, *MYB*, and other prominent regulators of AML cell fate (Supplementary Fig. S6P). A similar histone acetylation writer–reader module has also been described in AML, but on the level of enhancer regulation. H3K27ac is a critical mark of active enhancers, and it has been proposed that the p300/CBP HATs catalyze H3K27ac at *MYC* enhancers in AML cells, leading to recruitment of the acetyl-lysine reader BRD4 to promote high levels of transcription (35). These findings suggest that *MYC* can be regulated by multiple such transcriptional modules, all of which are of high therapeutic interest.

In addition to the KAT6A–ENL writer–reader module, we speculate that the H3K9 deacetylase SIRT1 may be a potential "eraser" in this process. Opposite to KAT6A, repression of SIRT1 induced a more "stem-like" AML state in our screen (Fig. 1B). Further, a recent study showed that MLL-r leukemias use DOT1L to prevent SIRT1 binding and maintain high promoter H3K9ac levels at AML oncogenes (75). As we have found an H3K9ac-dependent interrelationship between KAT6A, ENL, and other MLL-r transcriptional regulators such as DOT1L (Supplementary Fig. S5), it is possible that an additional function of this network is to cooperatively antagonize SIRT1-mediated H3K9 deacetylation.

We identified KAT6A via a screen for regulators of AML differentiation, and expression of the "core KAT6A target gene set" is highly correlated with expression of the LSC signature in patients with AML and cell lines. However, the KAT6A target genes and the LSC genes are largely nonoverlapping, suggesting that KAT6A may in fact regulate other upstream drivers of the LSC program rather than the LSC genes themselves. Interestingly, this is in line with a network-based analysis that predicted KAT6A as a potential master regulator upstream of the LSC gene regulatory model (76). Consistent with this possibility, we observed the most high-confidence direct KAT6A targets to include *MYC* and *MYB*, which are themselves thought to upregulate genes driving AML stemness and proliferation. It will be important in future studies to understand the KAT6A gene regulatory network in greater detail.

KAT6A may represent an actionable target of potential therapeutic interest in AML. Importantly, although KAT6A influences HSC activity, its loss in the hematopoietic system of adult mice is tolerated (77–79). Further, in the DepMap database, *KAT6A* KO is not detrimental to the growth of most cell types. Although KAT6A has been a challenging small-molecule inhibitor target, development of the WM-1119 and WM-8014 inhibitors that compete for KAT6A/B acetyl-coA binding represents a promising breakthrough. Improvements in inhibitor *in vivo* bioavailability will be needed to leverage their full potential. It will also be important to further determine the responsiveness of AMLs of different subtypes and mutational backgrounds to KAT6A inhibition. Our findings suggest that MLL-r AMLs may be the most sensitive to KAT6A loss. However, some non–MLL-r AML cell models had varying degrees of responsiveness as well.

KAT6A inhibitors may also be effective in combinatorial treatment schemes. Notably, development of ENL YEATS domain inhibitors would present the possibility of targeting both writer and reader of the described H3K9ac-focused AML transcriptional control module. Alternatively, as both KAT6A and BRD4 appear to promote *MYC* expression, their dual inhibition may represent a new method for more potent targeting of the MYC regulatory program. Another combinatorial possibility would entail targeting both drivers of stemness and proliferation as well as repressors of differentiation. Indeed, targeting of KAT6A and LSD1 showed marked promise in our preliminary combination treatment assays. It will next be of importance to test such possibilities in robust preclinical AML models.

In summary, we have identified a novel oncogenic transcriptional regulatory mechanism in AML that is driven by the HAT KAT6A. KAT6A is actionable and may serve as an attractive new therapeutic target for differentiation-based AML treatment.

METHODS

Mice

NSG mice used in this study were six-week-old female NSG mice purchased from The Jackson Laboratory (005557) and maintained in the mouse facility at the School of Veterinary Medicine at the University of Pennsylvania.

C57BL/6J mice used in this study were eight-week-old female mice purchased from The Jackson Laboratory (000664) and maintained in the mouse facility at the Center of Comparative Medicine at Massachusetts General Hospital. All mouse procedure protocols utilized in this study were in accordance with and with the approval of the Institutional Animal Care and Use Committee. All mouse experiment procedures used in this study were performed following the NIH guidelines.

Cells

Human AML cell lines (U937, MOLM-13, MV4;11, NOMO-1, MOLM-14, HL-60, OCI-AML3, and KG-1a) and a mouse RN2 AML cell line (a gift from Dr. Christopher Vakoc, Cold Spring Harbor Laboratories) were cultured in RPMI (Corning, 10-041-CV) with 10% FBS (Life Technologies, 16000044) and 1% penicillin–streptomycin (Gibco, 15-140-122). Mouse ER-HOXA9 and ER-HOXB8 cells were cultured in RPMI (Corning, 10-041-CV) with 10% FBS (Life Technologies, 16000044), 1% penicillin–streptomycin (Gibco, 15-140-122), 1% to 2% stem cell factor (SCF) conditioned media [generated from a Chinese hamster ovary (CHO) cell line that stably secretes SCF], and 0.5 μmol/L β-estradiol (Fisher Scientific, MP021016562). Mouse LSK-MLL–AF9 cells (a gift from Dr. Francois Mercier, McGill University) were cultured in RPMI (Corning, 10-041-CV) with 10% FBS (Life Technologies, 16000044), 1% penicillin–streptomycin (Gibco, 15-140-122), 1% to 2% SCF conditioned media (generated from a CHO cell line that stably secretes SCF), and 10 ng/mL IL3 (STEMCELL Technologies, 78042.1).

Mouse MLL–AF9 cells were generated through the following procedures: A female Cas9-GFP mouse (cat. #024828) was purchased from The Jackson Laboratory, and bone marrow was harvested from the femurs. Mononuclear bone marrow cells were collected by Ficoll-Paque plus density gradient centrifugation and placed into

culture (RPMI, with 10% FBS, 1% penicillin–streptomycin, SCF, IL3, and IL6, all at 10 ng/mL). Approximately 36 hours later, 250,000 cells (500 μL) were transduced with MSCV-based retrovirus expressing MLL/AF9-IRES-GFP (1 mL). This was done by spinfection (1,000 G, 22°C, 90 minutes) in the presence of polybrene (8 μg/mL). Media (3 mL; RPMI with 10% FBS, 1% penicillin–streptomycin, SCF 1% conditioned media, and 5 ng/mL IL3) were added following the spinfection. The following day, a half-media change was performed to further dilute out the polybrene. At approximately four weeks, the transduced cells had formed an immortalized population of GFP$^+$ cells expressing MLL–AF9. Five million cells were injected (retro-orbital) into a sublethally (450 cGy) irradiated mouse to establish a primary leukemia. Moribund mice were euthanized, and bone marrow leukemia cells were collected for future experiments, and maintained in culture in the same media containing SCF and IL3. The mouse Cas9–AML1-ETO cell line was a gift from Dr. Stephen Nimer (University of Miami).

All cell lines were tested for *Mycoplasma* contamination (and all confirmed *Mycoplasma* negative) routinely, including upon each unfreeze and then at least monthly during periods of continued culture. Testing was performed using the Universal Mycoplasma Detection Kit (ATCC, 30-1012K) according to the manufacturer's instructions.

Bone marrow or peripheral blood mononuclear cells from patients with AML (AML_6457, 7050, 7052) were obtained from the Stem Cell and Xenograft Core (SCXC) facility at the University of Pennsylvania. Samples were obtained by the Core after written informed consent. The SCXC tissue bank is approved under the University of Pennsylvania Institutional Review Board (IRB) protocol 703185, which is renewed annually. All samples are collected and distributed in accordance with recognized ethical guidelines as outlined by the Belmont Report and the U.S. Common Rule.

AML_010 (AML_2017_010) were obtained with written informed consent at Thomas Jefferson University Hospital in accordance with the Declaration of Helsinki and an IRB-approved protocol (#17D.083).

Human primary AML cells were cultured in Iscove's modified Dulbecco's medium (IMDM; Gibco, 12440-053) with 2% FBS (Life Technologies, 16000044) and 1% penicillin–streptomycin (Gibco, 15-140-122) at a concentration of 2 million cells/mL. Three days after drug treatment, live cells were isolated through FACS for RNA preparation and qPCR analysis.

Virus Packaging and Transduction

For lentivirus packaging, the target vector and pCMV-VSV-G and pCMV-dR8.2 dvpr lentiviral packaging plasmids (gifts from Dr. Bob Weinberg, Massachusetts Institute for Technology) Addgene plasmid #8454 and Addgene plasmid #8455, were cotransfected into 293T cells (Clontech, 632180) using PEI reagent (Polysciences, 23966-1). Lentiviral particles were collected 48 and 72 hours after transfection, filtered, and added to target cells with 8 μg/mL polybrene (Sigma, TR-1003-G). For retrovirus packaging, the target vector was transfected into the GPG29 packaging cell line using Lipofectamine 2000 (Invitrogen). Retroviral particles were collected 72 to 96 hours after transfection, filtered, and added to target cells with 8 μg/mL polybrene (Sigma, TR-1003-G). Transduced cells were then selected by appropriate antibiotics or cell sorting 48 hours after infection.

CRISPR–Cas9-Mediated Gene Targeting

The Cas9-expression vector lentiCas9-Blast was a gift from Dr. Feng Zhang at the Broad Institute of Harvard and MIT (Addgene plasmid #52962). Cas9 protein was introduced to human AML cell lines by lentiviral transduction and selected with 10 μg/mL Blasticidin (Thermo Fisher Scientific, R21001). The sgRNA-expression vectors LRG (Lenti_sgRNA_EFS_GFP; Addgene plasmid #65656) and LRCherry2.1 (Addgene plasmid #108099) were gifts from Dr. Christopher Vakoc. Cells were transduced with sgRNA lentivirus and sorted for GFP$^+$ cells 48 hours following transduction (except for the negative-selection competition assay). CRISPR sgRNA sequences used were:

sgKAT6A-1: CATACCACTGTTGCCACAGT; sgKAT6A-2: TTCGAGTGAAGGCCTTACGG;
sgKAT6A-3: CTCATCTCCTGTGCCGACTG; sgKAT6A-4: TTAGTGTTGAGCCGATAAAG;
sgKat6a-1: TGCAGCTCCTGTCGTGACCA; sgKat6a-2: GCTATTGCCGCAGTCCGCGC;
sgKat6a-3: CTCGTCTCCTGCGCGGACTG; sgKat6a-4: CGGCGCTATGCTAATCCAAT;
sgKat6a-5: TATGTCAGATATGCCGACCT; sgKat6a-6: CTCAATGCACTGCCACCGTA;
sgRosa26: GAAGATGGGCGGGAGTCTTC; sgNonTarget: ATTGAGAATTCGTTTCAAGG.

Except for the negative-selection competition assay that used all the sgRNAs, all other assays used human sgKAT6A-2 and mouse sgKat6a-6, if not otherwise indicated.

shRNA-Mediated Gene Knockdown

The shRNA-expression vector pLKO.1 puro was a gift from Dr. Bob Weinberg (Addgene plasmid #8453). Cells were transduced with shRNA lentivirus and then selected with 2 μg/mL puromycin. shRNA sequences used were:

shKAT6A-1: CCGCTGTCACAGTGTAGTATG; shKAT6A-2: ACAACAGCCACAACGTCTATA.

Gene Overexpression

Human WT and mutant *KAT6A* cDNA were cloned into a lentiviral EFS-P2A-mCherry expression vector (a gift from Dr. Junwei Shi, University of Pennsylvania; derivative of Addgene plasmid #108100 LentiV-Cas9-puro, where Cas9 was removed and puro was replaced by mCherry using the In-fusion cloning system; Clontech #638909). Cells were transduced with lentivirus and then sorted to obtain mCherry$^+$ cells.

Human WT *MYC* cDNA construct (lentiV-EFS-Flag-hMYC-PGK-Blast) was a gift from Dr. Junwei Shi. Cells were transduced with lentivirus and then selected with 10 μg/mL blasticidin.

Quantitative PCR Analysis for Gene Expression

Total RNA was prepared from AML cells using the RNeasy Mini Kit (Qiagen). cDNA was generated using the High-Capacity cDNA Reverse Transcription Kit (Applied Biosystems) from 1 μg RNA and diluted 1:10 for qPCR analysis. qPCR was performed using 2 μL diluted cDNA with biological and technical replicates using SYBR Green Master Mix (Applied Biosystems) with QuantStudio 3 real-time PCR system, and results were normalized to the expression of *ACTB/Actb*. Primer sequences utilized for qPCR were:

Human:
KAT6A-F: ATAATCCTGGGCGAATAGCACT; *KAT6A*-R: CTGCCTCCGAATAATGCAGAC;
MYC-F: ACCCTCTCAACGACAGCAGC; *MYC*-R: ACTCCGTCGAGGAGAGCAGA;
HOXA9-F: CCCCATCGATCCCAATAACCC; *HOXA9*-R: TTTGTATAGGGGCACCGCTT;
MEIS1-F: GGGCATGGATGGAGTAGGC; *MEIS1*-R: GGGTACTGATGCGAGTGCAG
ACTB-F: GCGGGAAATCGTGCGTGACATT; *ACTB*-R: CTAGAAGCATTTGCGGTGGA.

Mouse:
Kat6a-F: CCTCGTGCATTGGCTGTTC; *Kat6a*-R: TCATGGCATTCAAGGTGTTCAT;

Myc-F: GCATGAGGAGACACCGCCCA; *Myc*-R: GGTTTGCCTC TTCTCCACAGA;
Actb-F: AGTGTGACGTTGACATCCGT; *Actb*-R: TGCTAGGAGCC AGAGCAGTA.

In Vitro *Drug Treatment*

Cells were treated in triplicates and treated with indicated concentration of drugs or DMSO.

Chemicals used are listed below:

WM-8014, MedChemExpress, HY-102060
WM-1119, MedChemExpress, HY-102058
SAHA, Cayman, 10009929
EPZ-5676, MedChemExpress, HY-15593
5-Aza, Adooq Bioscience, A10105
Decitabine, Adooq Bioscience, A10292
ORY-1001, Cayman, 19136
SNDX-5613, MedChemExpress, HY-136175

Negative-Selection Competition Assay

AML cells were transduced with lentivirus expressing sgRNAs to achieve a roughly 50% transduction rate. The percentage of GFP^+ or $mCherry^+$ sgRNA-expressing cells was measured using flow cytometry over time and normalized to the percentage of GFP^+ or $mCherry^+$ cells on indicated start day.

Colony Formation Assay

Clonogenic potential was assessed by seeding the indicated number of cells in methylcellulose media.

For cell lines: to make 100-mL complete methylcellulose media, 40-mL methylcellulose base media (Stem Cell Technologies, MethoCult H4100) was supplemented with IMDM (Gibco, 12440-053), 10% FBS (Life Technologies, 16000044), 1% penicillin–streptomycin (Gibco, 15-140-122), and other desired supplements as described previously in cell culture section. The complete media were then used to resuspend the cells. The number of colonies was counted two weeks following seeding.

For human primary AML cells: to make 100-mL complete methylcellulose media, 75-mL methylcellulose base media (R&D Systems, #HSC005) was supplemented with IMDM (Gibco, 12440-053), 10% FBS (Life Technologies, 16000044), and 1% penicillin–streptomycin (Gibco, 15-140-122). The complete media were then used to resuspend the cells. The number of colonies was counted two weeks following seeding.

Flow Cytometry and Cell Sorting

For flow-cytometric analyses of cell-surface CD11b and CD86, cells were washed with PBS and then stained with PE-CD11b antibody (BioLegend, #101207) or FITC-CD86 antibody (BioLegend, #374203) at room temperature for 15 minutes and then washed twice with cold PBS for flow-cytometric analysis. For EdU (Life Technologies, #C10634), cell senescence (Thermo Scientific #C10840), and annexin V cell apoptosis (Life Technologies, #A23204) analyses, cells were prepared following product instructions and then analyzed by flow cytometry. Flow cytometry was performed on BD LSRFortessa (BD Biosciences) and analyzed with FlowJo software (Treestar). FACS of AML cells was performed by MoFlo Astrios (Beckman) or BD Jazz (BD Biosciences) according to the manufacturer's instructions.

Superoxide Anion Assay

A Superoxide anion assay was performed using Sigma #CS1000 kit following product instructions. Luminescence was measured using the EnVision (PerkinElmer) plate reader every 10 minutes for 4 hours.

Cell Viability Assay

Cells were harvested for cell viability assay six days after drug treatment. Cell viability assay was performed using CellTiter-Glo Luminescent Cell Viability Assay (Promega, #G7571) following product instructions. Luminescence was measured once using the EnVision (PerkinElmer) plate reader after 10 minutes of incubation.

Animal Experiments

For MOLM-13 cell transplantation: Cas9-expressing MOLM-13 cells were initially transduced with retrovirus of luciferase/GFP-expressing vector pSFG-NES-TGL (80). Cells were then transduced with an empty vector/sgRNA-expressing LRCherry2.1 plasmid. Two days following sgRNA transduction, GFP and mCherry double-positive AML cells were isolated via FACS. A total of 500,000 sorted cells per mouse were then transplanted by tail-vein injection into NSG mice that had been sublethally (2 Gy) irradiated 24 hours prior to injection ($n = 7$ mice per group). To quantify leukemia burden, bioluminescence imaging of mice was performed with an IVIS Spectrum In Vivo Imaging System immediately following retro-orbital injection of 200 μL (15 mg/mL) D-Luciferin (GoldBio, LUCK-1g) on the indicated days. Quantifications were performed using Living Image software (PerkinElmer) with whole-body total photon flux used as a readout for leukemic cell burden for each mouse at all timepoints.

Kaplan–Meier survival curves and log-rank tests were performed using Prism software (GraphPad). At the study endpoint, bone marrow and peripheral blood of sgKAT6A mice were harvested for flow cytometry of GFP and mCherry levels to identify KO-escaped leukemia cells.

For mouse MLL–AF9 cell transplantation: Cas9-GFP-expressing MLL–AF9 cells were transduced with an empty vector/sgRNA-expressing LRCherry2.1 plasmid. Transduced MLL–AF9 cells expressing both GFP and mCherry were sorted two days following transduction by FACS. A total of 500,000 cells per mouse from respective group were transplanted by retro-orbital injection into C57BL/6J mice that had been subjected to whole-body irradiation at a single sublethal dose of 4.5 Gy ($n = 5$ mice per group). In order to investigate leukemic burden of transduced MLL–AF9 cells, 21 days following transplantation, bone marrow of sgKat6a and control mice were harvested for flow cytometry of GFP leukemia cells.

Pooled CRISPR–Cas9 Screen and Screen Analysis

The human epi-RBP CRISPR sgRNA library was constructed using the methodology described in detail in a recent publication (81). Briefly, the sgRNA oligos were designed according to a published method (27), and 100 nontargeting control sgRNAs were also included. The sgRNA library was synthesized using array synthesis by CustomArray, Inc., and cloned as a pool into the lentiGuide-puro transfer plasmid via Gibson ligation reaction (NEB). After ligation, the library was transformed into electrocompetent cells (Lucigen) for amplification.

For the CRISPR screen, two biological replicates (independent transductions performed on different days) were performed and sequenced together. Cas9-expressing U937 AML cells were first transduced with the sgRNA lentivirus library at a multiplicity of infection of 0.2. At least 200× coverage of the sgRNA library in U937 cells was maintained throughout the screen. AML cells were sorted via FACS based on surface expression of CD11b into CD11b-high and CD11b-low samples for library preparation. Genomic DNA from sorted and bulk AML cells was harvested using the QIAamp DNA mini kit (Qiagen). Sequencing libraries were then prepared following previously described protocols (28). All prepared genomic DNA was used for library preparation for maintaining library coverage. PCR-amplified library samples were purified with the QIAquick PCR Purification Kit (Qiagen) followed by gel extraction with the QIAquick Gel Extraction Kit (Qiagen). The barcoded libraries were then pooled at an equal molar ratio and sequenced on a NextSeq500/550 (Illumina, 150 cycles High Output Kit v2.0) to generate 150-bp single-end reads. MAGeCK software was used for screen analysis (33). Briefly, the resulted sequencing data were debarcoded, merged, and the 20-bp

sgRNA sequence was aligned to the reference sgRNA library without allowing for any mismatches. The read counts were calculated for each sgRNA using the method normalizing to the nontargeting sgRNAs. Differential analysis of sgRNA and targeted genes was also done following the MAGeCK instructions with standard parameters. Detailed scripts and parameters used for each step of analysis could be provided by request to the authors.

RNA-seq Analysis

RNA samples of two to three biological replicates were extracted from cultured cells, using the Qiagen RNeasy Kit, following the manufacturer's instructions. RNA was then sent out for library preparation and next-generation sequencing to a commercial company, Novogene. Raw counts of gene transcripts were derived from raw fastq files using the alignment-independent quantification tool Salmon (https://combine-lab.github.io/salmon/), with standard settings. The raw count matrix was then imported into R-studio and utilized as input for DESeq2 analysis following the vignette of the package for normalization, differential gene-expression analysis, and unbiased clustering analysis, including principal component analysis (82). The output of DESeq2 was used as the input for preranked-based GSEA for enrichment of functional pathways and gene signatures (https://www.gsea-msigdb.org/gsea/index.jsp). Top differentially expressed genes were used as input for HOMER (−1,000 bp to +300 bp as scanning region) for the identification of motifs of potential transcriptional regulators (http://homer.ucsd.edu/homer/motif/). Detailed scripts and parameters used for each step of analysis could be provided by request to the authors.

ChIP-qPCR, ChIP-seq, and Analysis

Five to ten million cells were used for ChIP of each target. Cells were washed with PBS, cross-linked with 1% formaldehyde for 10 minutes at room temperature, and then quenched with 125 mmol/L glycine for five minutes. The isolated nuclei were resuspended in 1 mL nuclei lysis/sonication buffer and sonicated with Covaris S220 sonicator with the following parameters: peak intensity, 140; duty factor, 5; cycles per burst, 200; time, 60 seconds on, 30 seconds off for 16 cycles. After centrifugation at 4 degrees with 13,500 rpm for 10 minutes, soluble chromatin was then used to perform immunoprecipitation, whereas 5% sample was kept as input DNA. Immunoprecipitation was performed with 5 to 10 μg of the indicated antibodies overnight at 4°C with rotation. Products were then incubated with magnetic Protein G Dynabeads and then washed sequentially using low-salt, high-salt, LiCl buffer, and TE buffer. Bound DNA was then eluted, reverse-cross-linked, and incubated with RNase A and Proteinase K. DNA samples were purified using QIAquick PCR Purification Kit (Qiagen) and used for ChIP-qPCR or preparation of ChIP-seq libraries.

The following primers were used for ChIP-qPCR analysis:

Gene desert: Active motif #71001, human negative control primer set 1:
MYC transcription start site (TSS) + 1 kb-F: AAGGGAGGCGAG GATGTGT; R: TTCGCCCTGGTTTTTCCAA;
MYB TSS + 2 kb-F: GTGGGAATTCGTTCCGGGAT; R: ACTT GCAAAATGAGCCGCAG

ChIP-seq libraries were prepared following the NEBNext Ultra II DNA Library Prep Kit (New England Biolabs) protocol, using NEBNext Multiplex Oligos Index Primers Sets. Libraries were pooled and sequenced on the NextSeq500/550 (Illumina, 75 cycles High Output Kit v2.0) to generate 75-bp single-end reads or paired-end reads. Sequencing reads were aligned to the human (hg38) using Bowtie2 with default settings (83). Resulting sam files were filtered for uniquely aligned reads, converted to bam files, sorted, and marked for duplicated reads using SAMtools (84). Peak calling was performed using MACS2 with –nomodel –extsize 147 -q 0.1 for HA-KAT6A, FLAG-ENL, and histone marks (H3K9ac, H3K14ac, and H3K23ac) analysis. Peaks were subsequently merged using BEDTools, and read counts were calculated in the merged peaks for every sample (85). Bigwig files generated from bam files and big files from biological replicates were merged and normalized for genome track visualization as well as localization analysis using deepTools. The resulting count table was then used to identify differentially genomic regions with edgeR (86, 87). edgeR results were used for the identification of peak-associated genes using the BEDTools *closest* function. Differentially associated genes were used as an input for functional analysis using the online Metascape tool (54). Differential genomic regions were also transformed to bed files and used for genomic region annotation using the ChIP-seeker analysis tool (88). Overlap between different genomic regions was analyzed using BEDTools *intersect* function. Detailed scripts and parameters used for each step of analysis could be provided by request to the authors.

Antibodies are listed below:

Anti–histone H3 (acetyl K9), Abcam, ab4441
Anti–acetyl-histone H3 (Lys14; D4B9), Cell Signaling Technology, 7627
Anti–acetyl-histone H3 (Lys23), Millipore, 07-355
Anti-HA tag, Abcam, ab9110
Anti-ENL, Millipore, ABE2596

Gene-Expression Profiling Interactive Analysis

Expression of *KAT6A* across different types of cancer and normal tissues was analyzed using an online tool, GEPIA (http://gepia.cancer-pku.cn/; ref. 89).

Cancer Dependency Map Portal Data Analysis

The DepMap portal (https://depmap.org/portal/), the CRISPR (Avana) Public 20Q2 data set, as well as the Combined RNAi (Broad, Novartis, Marcotte) data set were used for the analysis. No samples were excluded from the data set in this analysis. Following the DepMap instruction, the dependency scores of annotated genes were downloaded and then plotted as dot plots. Pearson correlation was then calculated for all the plots using Prism.

Histone Extraction and LC/MS-MS

Histone peptides were prepared for mass spectrometry analysis as described previously (90). Briefly, cell pellets were lysed with nuclear isolation buffer (15 mmol/L Tris pH 7.5, 60 mmol/L KCl, 15 mmol/L NaCl, 5 mmol/L $MgCl_2$, 1 mmol/L $CaCl_2$, 250 mmol/L sucrose, 0.2% NP-40 alternative, 1 mmol/L DTT, 0.5 mmol/L AEBSF, 10 mmol/L sodium butyrate), and histones were extracted and chemically derivatized and then desalted by C18. Approximately 1 μg of peptide was loaded onto an in-house packed fused silica capillary, C18 column (75 μm × 30 cm, 2.4 μm ReproSil-Pur, Dr. Maisch GmbH). Buffer A (0.1% formic acid) and buffer B (80% acetonitrile, 20% H2O, 0.1% formic acid) were used to separate peptides based on hydrophobicity on a Dionex Ultimate 3000 RSLCnano high-performance liquid chromatographic system connected to a Q-Exactive HF (Thermo Scientific). A 65-minute two-step linear gradient (equilibrated with 4% of ACN for 2 minutes; eluted with 27.2% ACN for 44 minutes; washed with 72% of ACN for 5 minutes; reequilibrated with 1.6% ACN for 11 minutes) at a flow rate of 400 μL/minute was used, and eluting peptides were electrosprayed into the mass spectrometer. The Q-Exactive HF was programmed with a data-independent acquisition (DIA) method, including an MS survey scan range up to 1,100 m/z [60,000 MS1 resolution, automatic gain control (AGC) 1e6 ions, 50 ms max ion injection time], and DIA MS2 isolation windows for CID fragmentation (Normalized Collision Energy 25, 27.5, 30) of 50 m/z windows [15,000 MS1 resolution, automatic gain control (AGC) 5e5 ions, auto max ion injection

time]. Raw MS files were imported into EpiProfile to perform peak area integration of histone peptides (91). The MS proteomics data have been deposited to the ProteomeXchange Consortium (http://www.proteomexchange.org/) via the PRIDE (92) partner repository.

Immunoblotting

Cells were washed with PBS and lysed in RIPA lysis buffer with protease inhibitor cocktail. Lysates were heated to 95°C in SDS sample buffer, separated by SDS-PAGE, and transferred to nitrocellulose or PVDF membrane. Membranes were blocked in 5% nonfat milk in PBS with 0.1% Tween-20, probed with indicated primary antibodies and LI-COR secondary antibodies, and visualized using the Odyssey imaging system. Representative plot of two to four biological replicates are shown.

Antibodies used are listed below:

Anti–histone H3 (acetyl K9), Abcam, ab4441
Anti–acetyl-histone H3 (Lys14), Millipore, 07-353
Anti–acetyl-histone H3 (Lys23), Millipore, 07-355
Anti–histone H3, Abcam, ab1791
Anti–c-Myc, Abcam, ab32072
Anti–β-actin, Santa Cruz Biotechnology, sc-8432

Data Availability

Raw sequencing files were uploaded into Gene Expression Omnibus with the accession numbers GSE156947, GSE156948, GSE157039, GSE157041, GSE157042, and GSE165076.

Software and Statistical Analysis

PRISM software and R were used for data processing, statistical analysis, and result visualization (http://www.graphpad.com). The R language and environment for graphics (https://www.r-project.org) was used in this study for the bioinformatics analysis of the CRISPR screen, RNA-seq, and ChIP-seq data. The R packages used for all analyses described in this article were from the Bioconductor and CRAN. On graphs, bars represent either SD or SEM, as indicated in legends. For all figures, $P < 0.05$ was considered statistically significant; *, $P < 0.05$; **, $P < 0.01$; ***, $P < 0.001$.

Authors' Disclosures

P.J. Sung reports grants from the Leukemia & Lymphoma Society and the American Society of Hematology outside the submitted work. L. Wan reports personal fees from Bridge Medicines outside the submitted work. B.Z. Stanger reports personal fees from iTeos Therapeutics and grants from Boehringer Ingelheim outside the submitted work. D.B. Sykes reports personal fees and other support from Clear Creek Bio, other support from SAFI Biosolutions, and personal fees from Keros Therapeutics outside the submitted work. No disclosures were reported by the other authors.

Authors' Contributions

F. Yan: Conceptualization, data curation, software, formal analysis, investigation, methodology, writing–original draft, writing–review and editing. **J. Li:** Conceptualization, data curation, formal analysis, investigation, methodology, writing–original draft, writing–review and editing. **J. Milosevic:** Investigation. **R. Petroni:** Investigation. **S. Liu:** Investigation. **Z. Shi:** Investigation. **S. Yuan:** Investigation. **J.M. Reynaga:** Investigation. **Y. Qi:** Investigation. **J. Rico:** Data curation, software, and investigation. **S. Yu:** Investigation. **Y. Liu:** Investigation. **S. Rokudai:** Investigation. **N. Palmisiano:** Investigation. **S.E. Meyer:** Investigation. **P.J. Sung:** Methodology. **L. Wan:** Investigation. **F. Lan:** Investigation. **B.A. Garcia:** Investigation. **B.Z. Stanger:** Investigation. **D.B. Sykes:** Supervision, methodology, writing–review and editing. **M.A. Blanco:** Conceptualization, data curation, formal analysis, supervision, investigation, methodology, writing–original draft, writing–review and editing.

Acknowledgments

We would like to acknowledge members of the Blanco laboratory for technical support and scientific discussions. We would also like to acknowledge Martin Carroll, Gerd Blobel, and Peter Klein for helpful scientific discussions. We thank Junwei Shi and Zhendong Cao at the University of Pennsylvania for providing valuable cell lines and plasmids, and Stephen Nimer at University of Miami for providing valuable cell lines. We thank members of the flow cytometry and cell sorting resource laboratories at the Children's Hospital of Philadelphia and University of Pennsylvania for technical help with flow analysis and sorting. We thank Daniel Beiting and members of the Center for Host-Microbial Interactions for assistance with next-generation DNA sequencing. We thank members of the animal vivarium at the University of Pennsylvania for assistance with housing and maintenance of mice used in xenograft experiments. We also thank the Stem Cell and Xenograft Core (SCXC) facility at the University of Pennsylvania for primary human AML cells. This work was supported in part by an NCI K22 grant 1K22CA214849 (to M.A. Blanco), a Leukemia Research Foundation Hollis Brownstein Research Award (to M.A. Blanco), NIH grant R01-CA229803 (to B.Z. Stanger), and a Blavatnik Family Fellowship (to J. Li).

The costs of publication of this article were defrayed in part by the payment of page charges. This article must therefore be hereby marked *advertisement* in accordance with 18 U.S.C. Section 1734 solely to indicate this fact.

Received October 6, 2020; revised September 2, 2021; accepted November 15, 2021; published first December 1, 2021.

REFERENCES

1. Döhner H, Weisdorf DJ, Bloomfield CD. Acute myeloid leukemia. N Engl J Med 2015;373:1136–52.
2. Siegel RL, Miller KD, Jemal A. Cancer statistics, 2020. CA Cancer J Clin 2020;70:7–30.
3. Dombret H, Gardin C. An update of current treatments for adult acute myeloid leukemia. Blood 2016;127:53–61.
4. De Thé H. Differentiation therapy revisited. Nat Rev Cancer 2018;18:117–27.
5. Papaemmanuil E, Gerstung M, Bullinger L, Gaidzik VI, Paschka P, Roberts ND, et al. Genomic classification and prognosis in acute myeloid leukemia. N Engl J Med 2016;374:2209–21.
6. Ferrara F, Schiffer CA. Acute myeloid leukaemia in adults. Lancet 2013;381:484–95.
7. Warrell RP, de Thé H, Wang ZY, Degos L. Acute promyelocytic leukemia. N Engl J Med 1993;329:177–89.
8. Degos L, Dombret H, Chomienne C, Daniel MT, Micléa JM, Chastang C, et al. All-trans-retinoic acid as a differentiating agent in the treatment of acute promyelocytic leukemia. Blood 1995;85:2643–53.
9. Dang L, Yen K, Attar EC. IDH mutations in cancer and progress toward development of targeted therapeutics. Ann Oncol 2016;27:599–608.
10. Wouters BJ, Delwel R. Epigenetics and approaches to targeted epigenetic therapy in acute myeloid leukemia. Blood 2016;127:42–52.
11. Sun Y, Chen BR, Deshpande A. Epigenetic regulators in the development, maintenance, and therapeutic targeting of acute myeloid leukemia. Front Oncol 2018;8:41.
12. Pelish H, Liau B, Nitulescu I, Tangpeerachaikul A, Poss Z, Silva D, et al. Mediator kinase inhibition further activates super-enhancer-associated genes in AML. Nature 2015;526:273.
13. Sun Y, Zhou B, Mao F, Xu J, Miao H, Zou Z, et al. HOXA9 reprograms the enhancer landscape to promote leukemogenesis. Cancer Cell 2018;34:643–58.
14. Yang L, Rodriguez B, Mayle A, Park HJ, Lin X, Luo M, et al. DNMT3A loss drives enhancer hypomethylation in FLT3-ITD-associated leukemias. Cancer Cell 2016;29:922–34.
15. Lu R, Wang P, Parton T, Zhou Y, Chrysovergis K, Rockowitz S, et al. Epigenetic perturbations by Arg882-mutated DNMT3A potentiate

aberrant stem cell gene-expression program and acute leukemia development. Cancer Cell 2016;30:92–107.
16. Dawson MA, Prinjha RK, Dittmann A, Giotopoulos G, Bantscheff M, Chan WI, et al. Inhibition of BET recruitment to chromatin as an effective treatment for MLL-fusion leukaemia. Nature 2011;478:529–33.
17. Zuber J, Shi J, Wang E, Rappaport AR, Herrmann H, Sison EA, et al. RNAi screen identifies Brd4 as a therapeutic target in acute myeloid leukaemia. Nature 2011;478:524–8.
18. Shi J, Whyte WA, Zepeda-Mendoza CJ, Milazzo JP, Shen C, Roe JS, et al. Role of SWI/SNF in acute leukemia maintenance and enhancer-mediated Myc regulation. Genes Dev 2013;27:2648–62.
19. Bhagwat AS, Roe JS, Mok BYL, Hohmann AF, Shi J, Vakoc CR. BET bromodomain inhibition releases the mediator complex from select cis-regulatory elements. Cell Rep 2016;15:519–30.
20. Harris W, Huang X, Lynch J, Spencer G, Hitchin J, Li Y, et al. The histone demethylase KDM1A sustains the oncogenic potential of MLL-AF9 leukemia stem cells. Cancer Cell 2011;21:473–87.
21. Schenk T, Chen W, Göllner S, Howell L, Jin L, Hebestreit K, et al. Inhibition of the LSD1 (KDM1A) demethylase reactivates the all-trans-retinoic acid differentiation pathway in acute myeloid leukemia. Nat Med 2012;18:605.
22. Maes T, Mascaró C, Tirapu I, Estiarte A, Ciceri F, Lunardi S, et al. ORY-1001, a potent and selective covalent KDM1A inhibitor, for the treatment of acute leukemia. Cancer Cell 2018;33:495–511.
23. Alba M-D, Spencer G, Lynch J, Ciceri F, Williams E, Amaral F, et al. Enhancer activation by pharmacologic displacement of LSD1 from GFI1 induces differentiation in acute myeloid leukemia. Cell Rep 2018;22:3641–59.
24. Vinyard ME, Su C, Siegenfeld AP, Waterbury AL, Freedy AM, Gosavi PM, et al. CRISPR-suppressor scanning reveals a nonenzymatic role of LSD1 in AML. Nat Chem Biol 2019;15:529–39.
25. Wan L, Wen H, Li Y, Lyu J, Xi Y, Hoshii T, et al. ENL links histone acetylation to oncogenic gene expression in acute myeloid leukaemia. Nature 2017;543:265.
26. Erb MA, Scott TG, Li BE, Xie H, Paulk J, Seo HS, et al. Transcription control by the ENL YEATS domain in acute leukaemia. Nature 2017;543:270–4.
27. Shalem O, Sanjana NE, Hartenian E, Shi X, Scott DA, Mikkelsen TS, et al. Genome-scale CRISPR-Cas9 knockout screening in human cells. Science 2014;343:84–7.
28. Joung J, Konermann S, Gootenberg JS, Abudayyeh OO, Platt RJ, Brigham MD, et al. Genome-scale CRISPR-Cas9 knockout and transcriptional activation screening. Nat Protoc 2017;12:828–63.
29. Barbieri I, Tzelepis K, Pandolfini L, Shi J, Millán-Zambrano G, Robson SC, et al. Promoter-bound METTL3 maintains myeloid leukaemia by m6A-dependent translation control. Nature 2017;552:126–31.
30. Wang T, Yu H, Hughes NW, Chen WW, Lander ES, Sabatini DM. Gene essentiality profiling reveals gene networks and synthetic lethal interactions with oncogenic Ras. Cell 2017;168:890–903.
31. Tzelepis K, Koike-Yusa H, De Braekeleer E, Li Y, Metzakopian E, Dovey OM, et al. A CRISPR dropout screen identifies genetic vulnerabilities and therapeutic targets in acute myeloid leukemia. Cell Rep 2016;17:1193–205.
32. Chen CC, Li B, Millman SE, Chen C, Li X, Morris JP, et al. Vitamin B6 addiction in acute myeloid leukemia. Cancer Cell 2020;37:71–84.
33. Li W, Xu H, Xiao T, Cong L, Love MI, Zhang F, et al. MAGeCK enables robust identification of essential genes from genome-scale CRISPR/Cas9 knockout screens. Genome Biol 2014;15:554.
34. Giotopoulos G, Chan WI, Horton SJ, Ruau D, Gallipoli P, Fowler A, et al. The epigenetic regulators CBP and p300 facilitate leukemogenesis and represent therapeutic targets in acute myeloid leukemia. Oncogene 2016;35:279–89.
35. Roe JS, Mercan F, Rivera K, Pappin DJ, Vakoc CR. BET bromodomain inhibition suppresses the function of hematopoietic transcription factors in acute myeloid leukemia. Mol Cell 2015;58:1028–39.
36. Bernt KM, Zhu N, Sinha AU, Vempati S, Faber J, Krivtsov AV, et al. MLL-rearranged leukemia is dependent on aberrant H3K79 methylation by DOT1L. Cancer Cell 2011;20:66–78.
37. Champagne N, Pelletier N, Yang XJ. The monocytic leukemia zinc finger protein MOZ is a histone acetyltransferase. Oncogene 2001;20:404–9.
38. Huang F, Abmayr S, Workman J. Regulation of KAT6 acetyltransferases and their roles in cell cycle progression, stem cell maintenance, and human disease. Mol Cell Biol 2016;36:1900–7.
39. Borrow J, Stanton VP, Andresen JM, Becher R, Behm FG, Chaganti RSK, et al. The translocation t(8;16)(p11;p13) of acute myeloid leukaemia fuses a putative acetyltransferase to the CREB-binding protein. Nat Genet 1996;14:33–41.
40. Carapeti M, Aguiar RCT, Goldman JM, Cross NCP. A novel fusion between MOZ and the nuclear receptor coactivator TIF2 in acute myeloid leukemia. Blood 1998;91:3127–33.
41. Kitabayashi I, Aikawa Y, Yokoyama A, Hosoda F, Nagai M, Kakazu N, et al. Fusion of MOZ and p300 histone acetyltransferases in acute monocytic leukemia with a t(8;22)(p11;q13) chromosome translocation. Leukemia 2001;15:89–94.
42. Ley TJ, Miller C, Ding L, Raphael BJ, Mungall AJ, Robertson G, et al. Genomic and epigenomic landscapes of adult de novo acute myeloid leukemia. N Engl J Med 2013;368:2059–74.
43. Bolouri H, Farrar JE, Triche T, Ries RE, Lim EL, Alonzo TA, et al. The molecular landscape of pediatric acute myeloid leukemia reveals recurrent structural alterations and age-specific mutational interactions. Nat Med 2018;24:103–12.
44. Barretina J, Caponigro G, Stransky N, Venkatesan K, Margolin AA, Kim S, et al. The Cancer Cell Line Encyclopedia enables predictive modelling of anticancer drug sensitivity. Nature 2012;483:603–7.
45. Lonsdale J, Thomas J, Salvatore M, Phillips R, Lo E, Shad S, et al. The Genotype-Tissue Expression (GTEx) project. Nat Genet 2013;45:580–5.
46. Novershtern N, Subramanian A, Lawton LN, Mak RH, Haining WN, McConkey ME, et al. Densely interconnected transcriptional circuits control cell states in human hematopoiesis. Cell 2011;144:296–309.
47. Sheikh BN, Phipson B, El-Saafin F, Vanyai HK, Downer NL, Bird MJ, et al. MOZ (MYST3, KAT6A) inhibits senescence via the INK4A–ARF pathway. Oncogene 2015;34:5807–20.
48. Baell J, Leaver D, Hermans S, Kelly G, Brennan M, Downer N, et al. Inhibitors of histone acetyltransferases KAT6A/B induce senescence and arrest tumour growth. Nature 2018;560:253–7.
49. Xu Y, Man N, Karl D, Martinez C, Liu F, Sun J, et al. TAF1 plays a critical role in AML1-ETO driven leukemogenesis. Nat Commun 2019;10:1–15.
50. Shima H, Yamagata K, Aikawa Y, Shino M, Koseki H, Shimada H, et al. Bromodomain-PHD finger protein 1 is critical for leukemogenesis associated with MOZ-TIF2 fusion. Int J Hematol 2014;99:21–31.
51. Wang WT, Han C, Sun YM, Chen ZH, Fang K, Huang W, et al. Activation of the lysosome-associated membrane protein LAMP5 by DOT1L serves as a bodyguard for MLL fusion oncoproteins to evade degradation in leukemia. Clin Cancer Res 2019;25:2795–808.
52. van Galen P, Hovestadt V, Wadsworth MH, Hughes TK, Griffin GK, Battaglia S, et al. Single-cell RNA-seq reveals AML hierarchies relevant to disease progression and immunity. Cell 2019;176:1265–81.
53. Somervaille TCP, Matheny CJ, Spencer GJ, Iwasaki M, Rinn JL, Witten DM, et al. Hierarchical maintenance of MLL myeloid leukemia stem cells employs a transcriptional program shared with embryonic rather than adult stem cells. Cell Stem Cell 2009;4:129–40.
54. Zhou Y, Zhou B, Pache L, Chang M, Khodabakhshi AH, Tanaseichuk O, et al. Metascape provides a biologist-oriented resource for the analysis of systems-level datasets. Nat Commun 2019;10:1–10.
55. Tyner JW, Tognon CE, Bottomly D, Wilmot B, Kurtz SE, Savage SL, et al. Functional genomic landscape of acute myeloid leukaemia. Nature 2018;562:526–31.
56. Mckenzie MD, Ghisi M, Oxley EP, Ngo S, Cimmino L, Esnault C, et al. Interconversion between tumorigenic and differentiated states in acute myeloid leukemia. Cell Stem Cell 2019;25:258–72.
57. Meyers RM, Bryan JG, McFarland JM, Weir BA, Sizemore AE, Xu H, et al. Computational correction of copy number effect improves specificity of CRISPR-Cas9 essentiality screens in cancer cells. Nat Genet 2017;49:1779–84.

58. McFarland JM, Ho ZV, Kugener G, Dempster JM, Montgomery PG, Bryan JG, et al. Improved estimation of cancer dependencies from large-scale RNAi screens using model-based normalization and data integration. Nat Commun 2018;9:1–13.
59. Mueller D, Bach C, Zeisig D, Garcia-Cuellar MP, Monroe S, Sreekumar A, et al. A role for the MLL fusion partner ENL in transcriptional elongation and chromatin modification. Blood 2007;110:4445–54.
60. Zhu L, Li Q, Wong SHK, Huang M, Klein BJ, Shen J, et al. ASH1L links histone H3 lysine 36 dimethylation to MLL leukemia. Cancer Discov 2016;6:770–83.
61. Krivtsov AV, Evans K, Gadrey JY, Eschle BK, Hatton C, Uckelmann HJ, et al. A menin-MLL inhibitor induces specific chromatin changes and eradicates disease in models of MLL-rearranged leukemia. Cancer Cell 2019;36:660–73.
62. Zuber J, McJunkin K, Fellmann C, Dow LE, Taylor MJ, Hannon GJ, et al. Toolkit for evaluating genes required for proliferation and survival using tetracycline-regulated RNAi. Nat Biotechnol 2011;29:79–85.
63. Wang GG, Calvo KR, Pasillas MP, Sykes DB, Häcker H, Kamps MP. Quantitative production of macrophages or neutrophils ex vivo using conditional Hoxb8. Nat Methods 2006;3:287–93.
64. Sykes DB, Kfoury YS, Mercier E, Janzer A, Schreiber SL, Scadden DT, et al. Inhibition of dihydroorotate dehydrogenase overcomes differentiation blockade in acute myeloid leukemia article inhibition of dihydroorotate dehydrogenase overcomes differentiation blockade in acute myeloid leukemia. Cell 2016;167:171–86.
65. Simó-Riudalbas L, Pérez-Salvia M, Setien F, Villanueva A, Moutinho C, Martínez-Cardús A, et al. KAT6B is a tumor suppressor histone H3 lysine 23 acetyltransferase undergoing genomic loss in small cell lung cancer. Cancer Res 2015;75:3936–44.
66. Klein BJ, Jang SM, Lachance C, Mi W, Lyu J, Sakuraba S, et al. Histone H3K23-specific acetylation by MORF is coupled to H3K14 acylation. Nat Commun 2019;10:1–13.
67. Schaefer EW, Loaiza-Bonilla A, Juckett M, DiPersio JF, Roy V, Slack J, et al. A phase 2 study of vorinostat in acute myeloid leukemia. Haematologica 2009;94:1375–82.
68. Stein EM, Garcia-Manero G, Rizzieri DA, Tibes R, Berdeja JG, Savona MR, et al. The DOT1L inhibitor pinometostat reduces H3K79 methylation and has modest clinical activity in adult acute leukemia. Blood 2018;131:2662–9.
69. Sun W, Triche T, Malvar J, Gaynon P, Sposto R, Yang X, et al. A phase 1 study of azacitidine combined with chemotherapy in childhood leukemia: a report from the TACL consortium. Blood 2018;131:1145–8.
70. Mayer J, Arthur C, Delaunay J, Mazur G, Thomas XG, Wierzbowska A, et al. Multivariate and subgroup analyses of a randomized, multinational, phase 3 trial of decitabine vs treatment choice of supportive care or cytarabine in older patients with newly diagnosed acute myeloid leukemia and poor- or intermediate-risk cytogenetics. BMC Cancer 2014;14:69.
71. Bradner J, Hnisz D, Young R. Transcriptional addiction in cancer. Cell 2017;168:629–43.
72. Liang J, Prouty L, Williams BJ, Dayton MA, Blanchard KL. Acute mixed lineage leukemia with an inv(8)(p11q13) resulting in fusion of the genes for MOZ and TIF2. Blood 1998;92:2118–22.
73. MacPherson L, Anokye J, Yeung MM, Lam EYN, Chan YC, Weng CF, et al. HBO1 is required for the maintenance of leukaemia stem cells. Nature 2020;577:266–70.
74. Valerio DG, Xu H, Chen CW, Hoshii T, Eisold ME, Delaney C, et al. Histone acetyltransferase activity of MOF is required for MLL-AF9 leukemogenesis. Cancer Res 2017;77:1753–62.
75. Chen CW, Koche RP, Sinha AU, Deshpande AJ, Zhu N, Eng R, et al. DOT1L inhibits SIRT1-mediated epigenetic silencing to maintain leukemic gene expression in MLL-rearranged leukemia. Nat Med 2015;21:335–43.
76. Jung N, Dai B, Gentles AJ, Majeti R, Feinberg AP. An LSC epigenetic signature is largely mutation independent and implicates the HOXA cluster in AML pathogenesis. Nat Commun 2015;6:1–12.
77. Katsumoto T, Aikawa Y, Iwama A, Ueda S, Ichikawa H, Ochiya T, et al. MOZ is essential for maintenance of hematopoietic stem cells. Genes Dev 2006;20:1321–30.
78. Sheikh BN, Yang Y, Schreuder J, Nilsson SK, Bilardi R, Carotta S, et al. MOZ (KAT6A) is essential for the maintenance of classically defined adult hematopoietic stem cells. Blood 2016;128:2307–18.
79. Thomas T, Corcoran LM, Gugasyan R, Dixon MP, Brodnicki T, Nutt SL, et al. Monocytic leukemia zinc finger protein is essential for the development of long-term reconstituting hematopoietic stem cells. Genes Dev 2006;20:1175–86.
80. Ponomarev V, Doubrovin M, Serganova I, Vider J, Shavrin A, Beresten T, et al. A novel triple-modality reporter gene for whole-body fluorescent, bioluminescent, and nuclear noninvasive imaging. Eur J Nucl Med Mol Imaging 2004;31:740–51.
81. Shi Z, Xu S, Xing S, Yao K, Zhang L, Xue L, et al. Mettl17, a regulator of mitochondrial ribosomal RNA modifications, is required for the translation of mitochondrial coding genes. FASEB J 2019;33:13040–50.
82. Love MI, Huber W, Anders S. Moderated estimation of fold change and dispersion for RNA-seq data with DESeq2. Genome Biol 2014;15:550.
83. Langmead B, Salzberg SL. Fast gapped-read alignment with Bowtie 2. Nat Methods 2012;9:357–9.
84. Li H, Handsaker B, Wysoker A, Fennell T, Ruan J, Homer N, et al. The Sequence Alignment/Map format and SAMtools. Bioinformatics 2009;25:2078–9.
85. Quinlan AR, Hall IM. BEDTools: a flexible suite of utilities for comparing genomic features. Bioinformatics 2010;26:841–2.
86. McCarthy DJ, Chen Y, Smyth GK. Differential expression analysis of multifactor RNA-Seq experiments with respect to biological variation. Nucleic Acids Res 2012;40:4288–97.
87. Robinson MD, McCarthy DJ, Smyth GK. edgeR: a Bioconductor package for differential expression analysis of digital gene expression data. Bioinformatics 2009;26:139–40.
88. Yu G, Wang LG, He QY. ChIP seeker: an R/Bioconductor package for ChIP peak annotation, comparison and visualization. Bioinformatics 2015;31:2382–3.
89. Tang Z, Li C, Kang B, Gao G, Li C, Zhang Z. GEPIA: a web server for cancer and normal gene expression profiling and interactive analyses. Nucleic Acids Res 2017;45:W98–102.
90. Sidoli S, Bhanu NV, Karch KR, Wang X, Garcia BA. Complete workflow for analysis of histone post-translational modifications using bottom-up mass spectrometry: from histone extraction to data analysis. J Vis Exp 2016;2016:54112.
91. Yuan ZF, Sidoli S, Marchione DM, Simithy J, Janssen KA, Szurgot MR, et al. EpiProfile 2.0: a computational platform for processing Epiproteomics mass spectrometry data. J Proteome Res 2018;17:2533–41.
92. Martens L, Hermjakob H, Jones P, Adamsk M, Taylor C, States D, et al. PRIDE: the proteomics identifications database. Proteomics 2005;5:3537–45.